2018

High-resolution Infrared Spectroscopy of the v18 and v26 Bands of Trans-1,3-pentadiene

Minh Tran
Connecticut College, minhtran1013@gmail.com

High-resolution infrared spectroscopy of the ν_{18} and ν_{26} bands of *trans*-1,3-pentadiene

Minh N. Tran ‘18

Department of Chemistry, Connecticut College,

New London, CT 06320

Research Advisor: Jacob T. Stewart

Table of Contents

Acknowledgements

First and foremost, I would like to express my sincere gratitude to my research advisor, Professor Jacob Stewart, for his guidance, understanding and encouragement over the last two years. Jacob has provided me tremendous help and great advice not only on this honors thesis, but also on my career goals and future studies. Jacob is the best advisor I could ask for and he made my college experience much more worthwhile.

I would like to thank other members of the Stewart Research Group that I have worked with. Michael is a great labmate and I appreciate his help in building the lab setup. Thanks Marcus for coding programs that made the analysis much simpler.

In addition, I want to say thank to Professor Stanton Ching and Professor Marc Zimmer for your helpful feedback and suggestions. I also appreciate the support from other professors in the Department of Chemistry.

Last but not least, I would like to thank my family and friends for their unconditional support. To my sister, another “Minh Tran”, thanks for always pushing me forward, even if I resist. A huge thank you to my friends, Duc Chu and Olga Nikolaeva, for standing by my side. To my dear TVXQ and Louis, thanks to your inspiring work, I have enough motivation to go this far. I’m very fortunate to have those amazing people in my life.

Abstract

A high-resolution absorbance spectrum of *trans*-1,3-pentadiene was obtained using a quantum cascade laser-based spectrometer. All spectra were calibrated using a methanol reference spectrum generated by SpectraPlot using the HITRAN Database. The frequency uncertainty is estimated as 0.002 cm^{-1}. Two peaks at 976.69 and 1003.50 cm^{-1} were assigned to ν_{18} and ν_{26} bands respectively. Supporting calculations of the anharmonic vibrational frequencies and rotational constants were performed at the MP2/cc-pVTZ level of theory. Two specific motions were assigned to the vibrational modes ν_{18} and ν_{26}. A spectrum of the ν_{26} band was simulated to assign specific transitions to satellite bands of ν_{26}, which include multiple Q-branch peaks at the region of 984-999 cm^{-1} and 1009-1015 cm^{-1}. A strong peak at 1002.10 cm^{-1} was assigned to a hot band of the ν_{26} transition.

Introduction

1. Trans-1,3-pentadiene

Trans-1,3-pentadiene is an important conjugated diene that has been widely used in various applications and industries.[1] Due to the conjugated system, this compound is very reactive to polymerization, which makes it a useful monomer. *Trans*-1,3-pentadiene can be used as an intermediate monomer in the production of plastics and adhesives, which include tapes and natural rubbers.[2, 3] This compound is also generated in the production of gasoline, which involves catalytic and thermal cracking of heavy petroleum fractions.[4, 5]

While *trans*-1,3-pentadiene is a simple molecule, it is a representative of the class of conjugated organic systems. Studies of this molecule can provide information and methods to understand other molecules of similar properties. This study mainly focused on the spectroscopic properties of *trans*-1,3-pentadiene. We acquired a high-resolution spectrum of *trans*-1,3-pentadiene and compared it with computational models. Comparison of the experimental data with computational calculations can estimate how accurate the calculations are and how close the calculations can predict properties of other molecules.

Spectroscopic properties of *trans*-1,3-pentadiene have been studied by both vibrational and rotational spectroscopy.[6, 7] A vibrational spectrum of the molecule was recorded over a range of temperatures for three phases in the previous work by Compton and George.[6] All vibrational modes were reported and assigned to specific vibrational motions.[6] The rotational constants were determined in the studies by Hsu and Flygare, which focuses on the microwave spectra of *trans*-1,3-pentadiene.[7] While there are high-resolution microwave spectra of this compound, there is no source for high-resolution infrared spectra. In this study, the first high-resolution infrared spectrum

of *trans*-1,3-pentadiene was obtained in the region of the ν_{26} vibrational mode near 1003.5 cm^{-1}. We also compared our experimental spectrum to anharmonic vibrational frequencies and rotational constants calculated using second-order perturbation theory. The high-resolution spectrum provides fundamental information about this vibrational band which will be useful for future efforts to monitor *trans*-1,3-pentadiene using infrared spectroscopy.

2. Quantum cascade laser

Semiconductor lasers have important applications in various fields, including molecular spectroscopy, atomic optics and interferometry.[8] With a wide variety of semiconductors, different types of lasers have been developed to provide new methods of research. Diode lasers are the simplest semiconductor lasers. A diode laser works as a p-n junction biased in the forward direction.[9] As the current flows through the semiconductor diode, electrons in the conduction band recombine with holes in the valence band, which generates emission of light.[8, 9] The radiative process dominates if two bands are close enough and the current is sufficiently large.[10] The frequency of the emitted radiation depends on the energy gap between the conduction and valence band of the semiconductor material. As a result, the major disadvantage of a diode laser is limited frequency range.[9]

The quantum cascade laser (QCL) is a special type of semiconductor laser which has a broader wavelength range and better control of emitted light compared to the diode laser. It was first demonstrated in 1994 as a compact mid-infrared source.[11] The QCL has only one type of carriers (unipolar semiconductor laser), and instead of depending on the energy gap between two electronic bands, it relies on the electron transitions between the quantized energy levels of the conduction band.[11, 12] The QCL consists a series of repeated thin layers of varying materials, which forms a superlattice.[13] The superlattice introduces a varying electric potential to the device so the

probability of electrons in different positions can be controlled, which is referred to as multiple quantum well confinement.[14] The bands of certain energies are split into discrete electronic sub-bands.[14] By suitable design of the layer thickness, it is possible to engineer a population inversion between two sub-bands in a series of identical repeated units to achieve laser emission.[14] The frequency of emitted radiation depends on the energy gap between sub-bands, which is determined by the layer thickness. As a result, the emission wavelength of QCLs can be tuned over a wide range in the same material system.[14]

QCLs are designed based on the multistage cascade scheme, which allows one charge carrier to lead to the generation of multiple photons.[15] Electrons entering the quantum well are trapped in an upper energy state.[15] They are stimulated to emit radiation and drop to a lower energy level. Electrons can tunnel out to the next quantum well, drop to another lower energy level and emit radiation.[15] By using multiple quantum wells (a cascade), more photons per electron are obtained as the electrons drop successively lower in energy as they pass along the structure (Figure 1).[15] This leads to a high quantum efficiency and a high optical output power because the number of photons and carriers is proportional to the number of stages.[15]

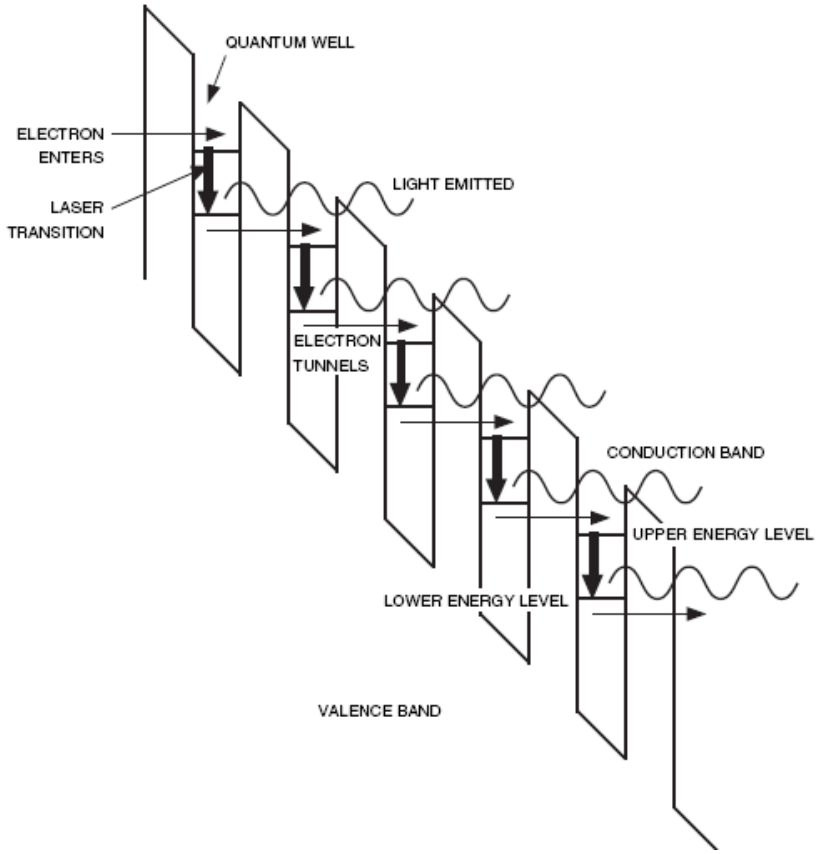

Figure 1. A simplified diagram of a quantum cascade laser. In QCLs, electrons undergo intersubband transitions and emit radiation. The electrons can tunnel to the next quantum well and the same process repeats.[15]

Since QCLs are powerful sources of emitting radiation, they have been used for various applications, including metrology, warfare chemical agent detection and trace gas sensing.[16] In this experiment, we use a QCL to study the ro-vibrational spectroscopy of *trans*-1,3-pentadiene.

3. Rotational spectroscopy

Absorption of electromagnetic radiation can cause molecules to rotate through the interactions of the electric dipole moments of the molecules and the electromagnetic field. The energies of rotational transitions correspond to microwave radiation, which has a wavelength in the range of

0.1 cm (300 GHz) to 100 cm (300 MHz). Rotational motion can be explained using the rigid rotator model for a diatomic molecule.[17] The Schrodinger equation of diatomic molecules can be solved exactly, which can be used as a basis to understand spectra of polyatomic molecules.

3.1 The rigid rotator model of a rotating diatomic molecule

A molecule rotating at a distance r from a fixed center has moment of inertia equals to μr^2, in which μ is the reduced mass.[17] While the moment of inertia expresses an object's tendency to resist motion, momentum is the quantity of motion of a moving body. The angular momentum, L, equals to:

$$L = I\omega \quad (3.1)$$

in which L is the angular momentum and ω is the angular speed.[17]

The kinetic energy is given by the following equation:

$$K = \frac{1}{2} I\omega^2 = \frac{L^2}{2I} \quad (3.2)$$

By solving Schrodinger equation, the energy of each rotational level is equivalent to

$$E_J = \frac{\hbar^2}{2I} J(J+1) \quad (3.3)$$

In which *J* is a quantum number and obtains positive integer values from 0 (J=0, 1, 2,…).[17]

The rotational constant, B, is defined as:

$$B = \frac{\hbar^2}{2I} \quad (3.4)$$ [18]

The energy can be expressed in terms of rotational constant:[18]

$$E_J = BJ(J+1) \quad (3.5)$$

The selection rule for the rigid rotator is that transitions are allowed only between adjacent states or $\Delta J = \pm 1$.[17] The degeneracy for each energy level is 2J+1. The intensity of a rotational transition depends on the dipole moment and the population difference between the two levels.[18] With the selection rule $\Delta J = \pm 1$, the frequency of a rotational transition is:

$$\nu_{J \to J+1} = 2B(J+1) \quad (3.6)$$

In which J= 0, 1, 2, … [18]

When a molecule rotates, the atoms experience a centrifugal force in the rotating molecular reference frame which distorts the internuclear positions.[18] The centrifugal distortion constant, D, can be added to equation (3.5) to account for the deviation of a molecule from the rigid rotator.[18]

3.2 Rotational spectroscopy of polyatomic molecules

A polyatomic molecule can be modeled as a rigid network of N atoms.[17] In a polyatomic molecule, when an atom rotates at a fixed distance from the center of mass, it has three angular velocities, ω_x, ω_y and ω_z, which are set to arbitrary orthonormal x, y and z axes intersecting at the center of mass.[19] Similar to the moment of inertia in diatomic molecules, polyatomic molecules have the moment of inertia tensor, I, which has the form of a matrix:

$$I = \begin{matrix} I_{xx} & I_{xy} & I_{xz} \\ I_{xy} & I_{yy} & I_{yz} \\ I_{xz} & I_{yz} & I_{zz} \end{matrix} \quad (3.7)$$ [18]

In general, the rotational kinetic energy contains three diagonal terms which are proportional to ω_x^2, ω_y^2 and ω_z^2.[19] Depending on the symmetry of the molecule, three principal axes, a, b and c, are specifically chosen so that the off-diagonal terms go to zero. If xyz axes rotate into a new body-fixed coordinate system with orthogonal axes a, b and c, the matrix becomes:

$$I = \begin{matrix} I_a & 0 & 0 \\ 0 & I_b & 0 \\ 0 & 0 & I_c \end{matrix} \quad (3.8)\ ^{19}$$

The kinetic energy expression is

$$K = \frac{1}{2}(I_a\omega_a^2 + I_b\omega_b^2 + I_c\omega_c^2) \quad (3.9)$$

By solving the Schrodinger equation as in diatomic molecules, three rotational constants A, B and C are obtained.

$$A = \frac{\hbar^2}{2I_a} \quad (3.10)$$

$$B = \frac{\hbar^2}{2I_b} \quad (3.11)$$

$$C = \frac{\hbar^2}{2I_c} \quad (3.12)$$

The relative magnitudes of the three principal moments of inertia can be used to characterize a rigid body.[17] By convention, the principal axes a, b and c are labeled so that rotational constants are ordered in decreasing magnitude:

$$A \geq B \geq C$$

For *trans*-1,3-pentadiene, two of the axes, a and b, lie in the plane of symmetry and c-axis is perpendicular to it (Figure 2).

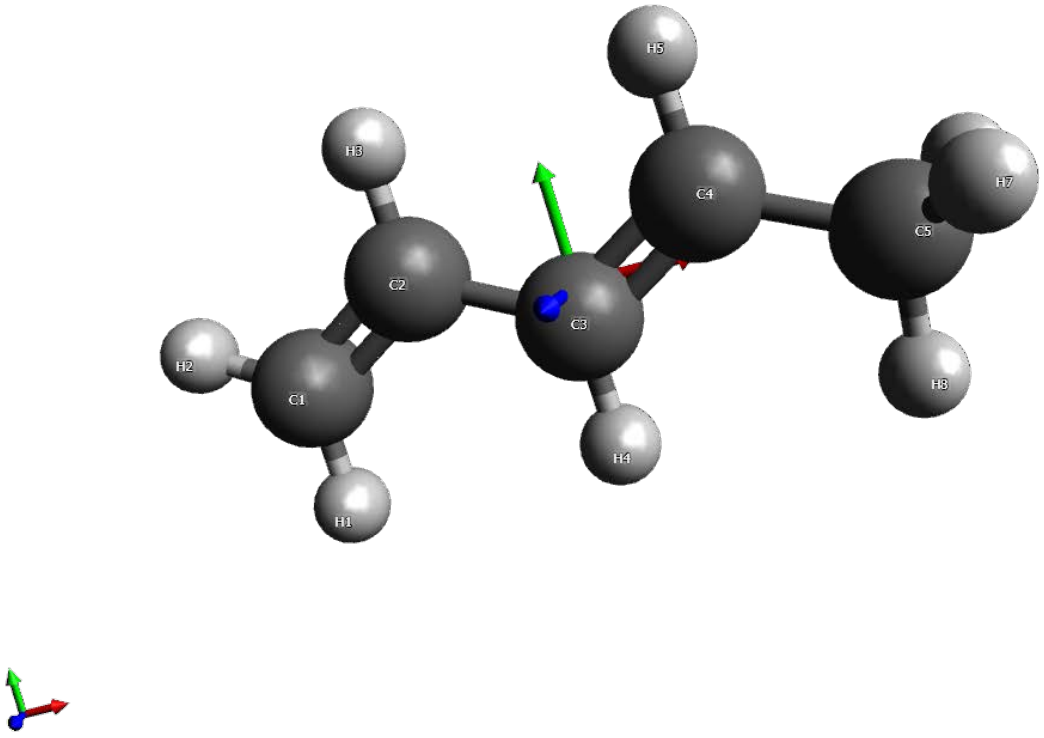

Figure 2. Three axes of *trans*-1,3-pentadiene. Red, green, blue axes denote a, b, c axes respectively.

Molecules can be classified on the basis of the values of three rotational constants or the moments of inertia: [18, 19]

Linear molecule: B = C or $I_A = 0$, $I_B = I_C$; example: HCN

Spherical tops: A = B = C or $I_A = I_B = I_C$; example: CH_4 and SF_6

Prolate symmetric tops: A > B = C or or $I_A < I_B = I_C$; example: CH_3Cl

Oblate symmetric tops: A = B > C or or $I_A = I_B < I_C$; example: BF_3

Asymmetric tops: A > B > C or $I_A < I_B < I_C$; example: H_2O

Trans-1,3-pentadiene has point group of C_s and is an asymmetric top. The Schrodinger equation for the asymmetric top has no general analytical solutions and must be solved with the help of computers.[18] For simplification, *trans*-1,3-pentadiene can be treated as a near-prolate symmetric top. Three rotational constants of *trans*-1,3-pentadiene reported from previous work of Hsu and Flygare show that the values of B and C are almost equal (A = 28.2 ±0.7GHz, B = 2160.61 ± 0.01 MHz and C = 2033.21 ±0.01 MHz).[7]

Solving the Schrodinger equation using the symmetric top wavefunction, the energy level of prolate tops and oblate tops can be expressed as: [18]

$E_{J\,K_a} = BJ(J+1) + (A-B)K_a^2$ (prolate top) (3.13)

$E_{J\,K_c} = BJ(J+1) + (C-B)K_c^2$ (oblate top) (3.14)

In which K_a and K_c are quantum number. K_a, K_c = 0, 1, 2,…

Since *trans*-1,3-pentadiene is treated as a near-prolate top, its energy level will be close to the expression for a prolate top (equation 3.13).

The selection rules for symmetric tops are

$\Delta J = 0, \pm 1$ and $\Delta K = 0$ for $K \neq 0$

$\Delta J = \pm 1$ and $\Delta K = 0$ for $K = 0$

And $J \geq K$.[17, 18]

While *trans*-1,3-pentadiene is treated as a near-prolate top for simple calculation, it is actually asymmetric top so transitions of other selection rules are also observed. The energy equation of an asymmetric top contains three quantum numbers, J, K_a and K_c and the selection rules depend on

three dipole moment components, μ_a, μ_b and μ_c along the principal axes.[18] The selection rule for J is $\Delta J = 0, \pm 1$ while the selection rules for K_a and K_c fall into three types of transitions:

a-type transition: $\mu_a \neq 0$, $\mu_b = \mu_c = 0$: $\Delta K_a = 0$ (±2, ±4,…) $\Delta K_c = \pm 1$ (±3, ±5,…)

b-type transition: $\mu_b \neq 0$: $\Delta K_a = \pm 1$ (±3, ±5,…) $\Delta K_c = \pm 1$ (±3, ±5,…)

c-type transition: $\mu_b \neq 0$: $\Delta K_a = \pm 1$ (±3, ±5,…) $\Delta K_c = 0$ (±2, ±4,…)

The transitions in parentheses are weaker than the main ones.[18]

Centrifugal distortion terms can also be added to account for the distortion of the molecule when it rotates.

4. Vibrational Spectroscopy

4.1 The harmonic oscillator model of diatomic molecules

The vibrational motion of diatomic molecules can be approximated as a harmonic oscillator.[17] The wave functions and energies of the quantum-mechanical harmonic oscillator can be used to describe the infrared spectrum of molecules.[17] Solving the Schrodinger equation for diatomic molecules can provide the basis to study polyatomic molecules.

The Schrodinger equation of a harmonic oscillator is:

$$-\frac{h^2}{2\mu}\frac{d^2\Psi}{dx^2} + V(x)\Psi(\mathrm{x}) = E\Psi(\mathrm{x}) \quad (4.1)$$

In which V(x) is the potential energy of the system and V(x) equals to $\frac{1}{2}kx^2$.[17]

By solving the Schrodinger equation, the energy equation can be expressed as quantum values:

$$E_v = h\nu\,(v + \frac{1}{2}) \quad (4.2)$$

where ν is the fundamental frequency and is equal to

$$\nu = \frac{1}{2\pi}\left(\frac{k}{\mu}\right)^{\frac{1}{2}} \quad (4.3)$$

and v is the quantum number, v = 0, 1, 2,…and μ is the reduced mass.[17]

The selection rule is $\Delta v = \pm 1$. Equation 4.2 indicates that the energy levels are equally spaced, with a separation of hν (Figure 3).[17]

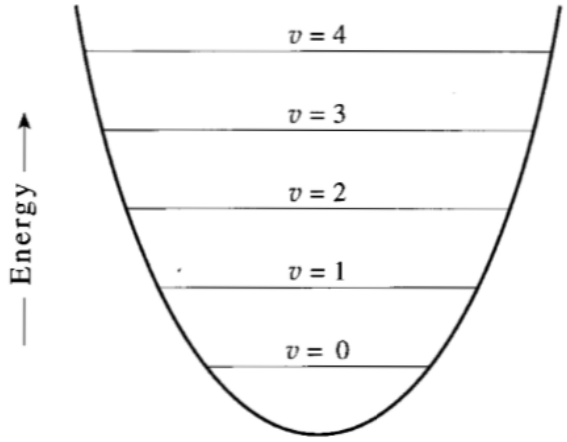

Figure 3. The energy levels of a harmonic oscillator are equally spaced.[17]

Since the energy levels are equally spaced and molecules can jump from one vibrational state to another by absorbing electromagnetic radiation, the observed frequency of any transition satisfies the following equation:

$$\Delta E = h\nu_{obs} \quad (4.4)$$

The observed frequency of the absorbed radiation is defined in the equation 4.3. The dipole moment of the molecule must change when it vibrates if the molecule absorbs infrared radiation.[17]

4.2 Vibrational Spectroscopy of polyatomic molecules

The harmonic oscillator approximation can be adjusted to discuss vibrational motions in polyatomic molecules. A molecule with N nuclei requires three coordinates for each nucleus, so it has 3N coordinates, or 3N degrees of freedoom.[17] Three coordinates specify the center of mass of the molecule, and motion along these three coordinates are translational degrees of freedom.[17] Three coordinates are used to specify the orientation of nonlinear molecules, which corresponds to rotational degrees of freedom.[17] The remaining 3N-6 coordinates specify the relative positions of the N nuclei.[17] For nonlinear molecules, there are three translational degrees of freedom, three rotational degrees of freedom and 3N-6 vibrational degrees of freedom. Since the energy does not depend on the position of the center of mass or its orientation, the potential energy is given by the following equation:

$$\Delta V = V(q_1, q_2, \dots, q_N) - V(0,0, \dots, 0) = \frac{1}{2}\sum_{i=1}^{N_{vib}} \sum_{j=1}^{N_{vib}} f_{ij} q_i \, q_j \quad (4.5)$$

In which $q_1, q_2, \dots, q_N$ are the displacements of the coordinates about the equilibrium values and N_{vib} is the number of vibrational degrees of freedom.[17]

By using a matrix to find a new set of coordinates $\{Q_i\}$, the potential energy can be expressed as:

$$\Delta V = \frac{1}{2}\sum_{j=1}^{N_{vib}} F_j Q_j^2 \quad (4.6)$$

In which Q_j is the matrix of set of coordinates.[17]

These new coordinates are called normal modes.[17] Normal modes describe the motions of atoms in a molecule and each mode is characterized by a different type of vibrational motion.

The vibrational Hamiltonian operator is

$$H_{vib} = -\sum_{j=1}^{N_{vib}}(-\frac{\hbar}{2\mu_j}\frac{d^2}{dQ_j^2} + \frac{1}{2}\sum_{j=1}^{N_{vib}} F_j Q_j^2) \quad (4.7)$$

By solving the Schrodinger equation, the vibrational energy of polyatomic molecules is

$$E_{vib} = \sum_{j=1}^{N_{vib}} h\nu_j \ (v_j + \frac{1}{2}) \quad (4.8)$$

Where each $\nu_j$is the quantum number, ν = 0, 1, 2,…[17]

Trans-1,3-pentadiene has 33 vibrational degrees of freedom so its vibrational energy can be express as:

$$E_{vib} = \sum_{j=1}^{33} h\nu_j \ (v_j + \frac{1}{2}) \quad (4.9)$$

The selection rule is Δv= ±1. Equation 4.9 shows that the vibrational motion of polyatomic molecules can be treated as N_{vib} independent harmonic oscillators, each with its own fundamental frequency ν_j.[17]

In the harmonic oscillator approximation, the bond length is assumed to be fixed. However, when the molecules vibrate, the bond length will change. When the bond length reaches its maximum, further stretching will break the bond. The potential energy at large separation is essentially the bond energy.[17] Anharmonic terms can be added to the potential energy expression to account for the difference between the molecule and the harmonic oscillator. For small quantum numbers, the difference between the harmonic and anharmonic wave functions are small so the harmonic oscillator model provides a good approximation.[18] When v increases, the amplitude of the anharmonic wave function increases so it cannot be neglected.[18] Also, due to the anharmonicity,

the energy levels are no longer equally spaced and the energy difference becomes smaller with increasing v (Figure 4).[17]

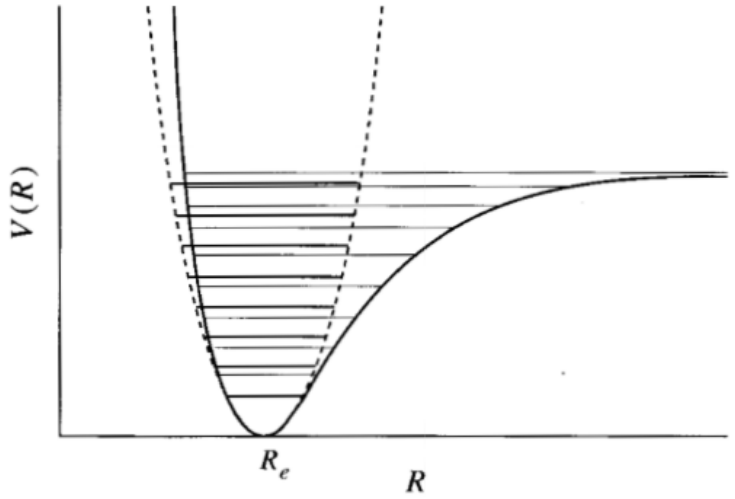

Figure 4. The deviation of energy levels of an anharmonic oscillatiors from a harmonic oscillator.[17]

If anharmonic wave functions are included, the transitions with Δv= ±2, ±3,… are also allowed.[18] Three main types of infrared transitions are the fundamental, overtone and hot bands. The transition v =0 -> v =1 is called the fundamental, while any transition with v =j -> v =j+1 (j ≠0) is called hot band (Figure 5).[18] These transitions are called hot bands because the intensities of these bands are larger when the temperature increases.[18] When the sample is heated, the molecules are excited and there is a higher number of molecules in the excited states than at room temperature where most molecules are in the ground state. The excited molecules can absorb infrared radiation and jump to a higher vibrational state, which is the hot band transition. Overtones occur when the selection rule is Δv= ±2, ±3,… When molecules are excited from v =0 to v =2, this transition is called first overtone; v =0 to v = 3 will be the second overtone and so on (Figure 5).[18] The intensities of overtone transitions decrease with increasing Δv.[18] At room temperature, the fundamental transitions with Δv= ±1 are the most common transitions.

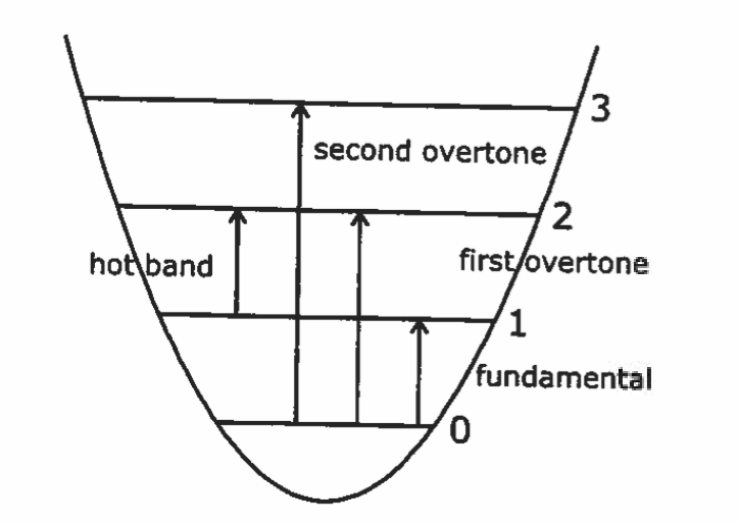

Figure 5. Three main types of vibrational transitions including fundamental, hot band and overtone.[18]

There are six types of vibration motions in polyatomic molecules: asymmetric and symmetric stretching, wagging, twisting, scissoring, and rocking (Figure 6). For molecules with C_s point group, in-plane and out-of-plane vibrations are denoted as A' and A'' respectively.

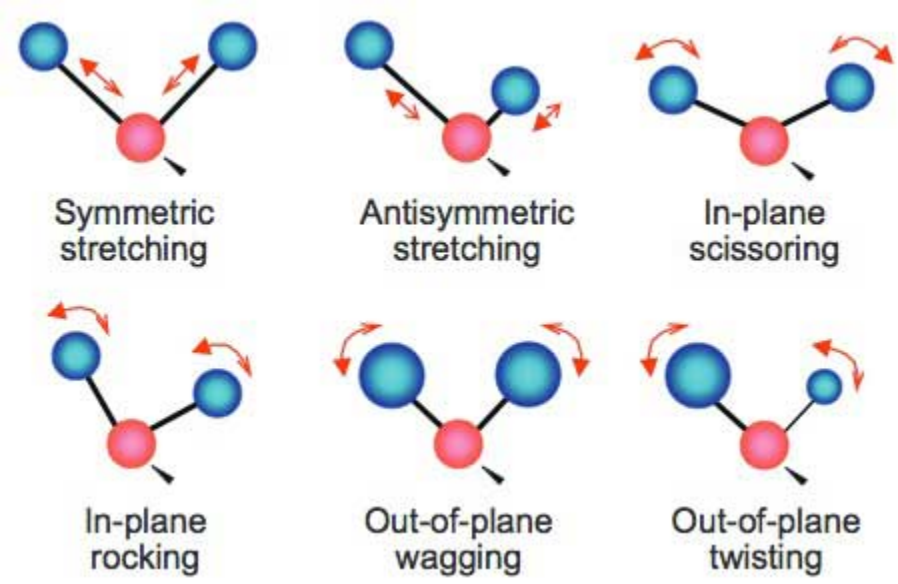

Figure 6. Six types of vibrational motions.[20]

Previous studies by Compton and George assigned 33 vibrational modes of *trans*-1,3-pentadiene to specific motions and their corresponding fundamental frequencies in wavenumbers.[6]

4.3 Ro-vibrational Spectroscopy

When molecules absorb infrared radiation, rotational transitions accompany the vibrational transitions (Figure 7).[17]

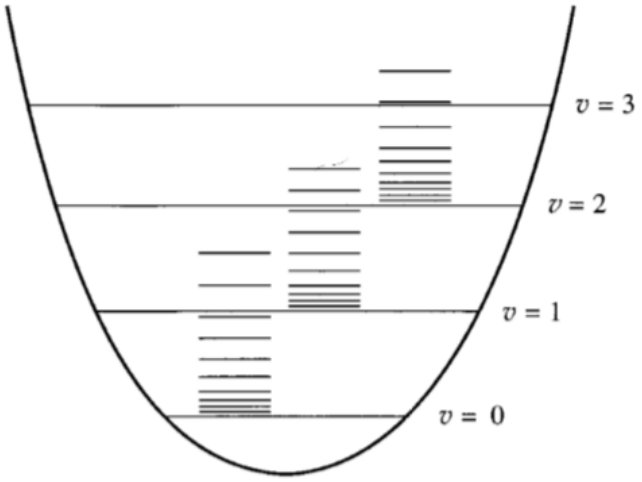

Figure 7. Rotational transitions accompany with vibrational transitions.[17]

The selection rules for absorption of infrared radiation are $\Delta v = +1$ and $\Delta J = 0, \pm 1$. Transitions with $\Delta J = 0$ are called the Q-branch. Transitions with $\Delta J = +1$ and $\Delta J = -1$ belong to the R-branch and P-branch respectively. The R-branch has highest frequency and P-branch has lowest frequency because the rotational state increases in R-branch and decreases in P-branch.[17] An example of the infrared spectrum of C_2H_4 is provided with the relative position of P, Q and R-branchesF.

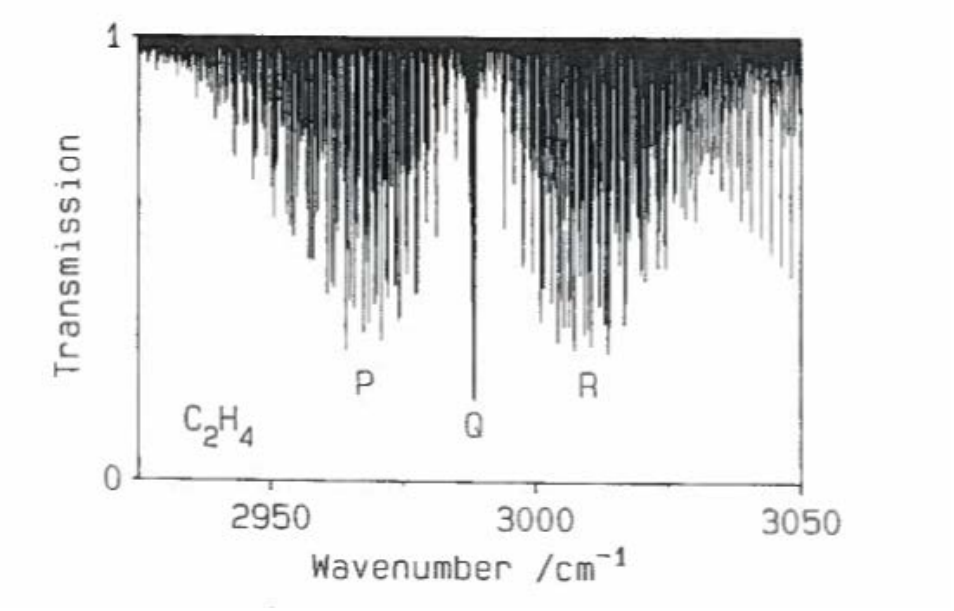

Figure 8. Infrared spectrum of ethylene. [18]

The ro-vibrational transitions of asymmetric tops can also be classified as a-type, b-type transition, and c-type, with the selection rules as same as microwave transitions.[18]

Experimental

1. QCL Spectrometer

A quantum cascade laser (QCL)-based spectrometer was built to obtain high-resolution infrared spectra of *trans*-1,3-pentadiene (Figure 9). The light source of this system is a mode hop free external cavity QCL from Daylight Solutions which has a tuning range of 962-1019 cm^{-1} and operates with a linewidth of ~0.0003 cm^{-1} over a 1 second integration time. The light from the QCL is split into two directions by a ZnSe beamsplitter (ThorLabs, BSW710). Half of the light is sent through a multipass absorption cell (Aerodyne Research, AMAC-76), which contains the *trans*-1,3-pentadiene sample. The multipass cell has small, circular mirrors on two sides, which can reflect the laser as it comes in multiple times before going to the detector. A longer path length increases the absorbance, which allows us to obtain higher signals at lower sample concentration. The light coming out from the multipass cell is detected by a thermoelectrically cooled MCT detector (Vigo Systems, PVI-2TE10.6-1x1). The remaining light goes through a reference cell (CRD Optics, 0.5-m Sample Cell 903-0001) containing a low pressure of pure methanol (< 10 torr). The light is detected by a room-temperature photovoltaic MCT detector (Vigo Systems, PVM-10.6-1x1). Signals from the detectors are digitized by a data acquisition card (LabJack, U6) at a rate of 4 kHz and saved onto a personal computer.

The multipass cell is connected to a system which contains a vacuum pump, a pressure gauge (MKS Instruments, 722A12TBA2FA) and a removable glass bulb (Chemglass Airfree). This system helps to transfer *trans*-1,3-pentadiene to the multipass cell.

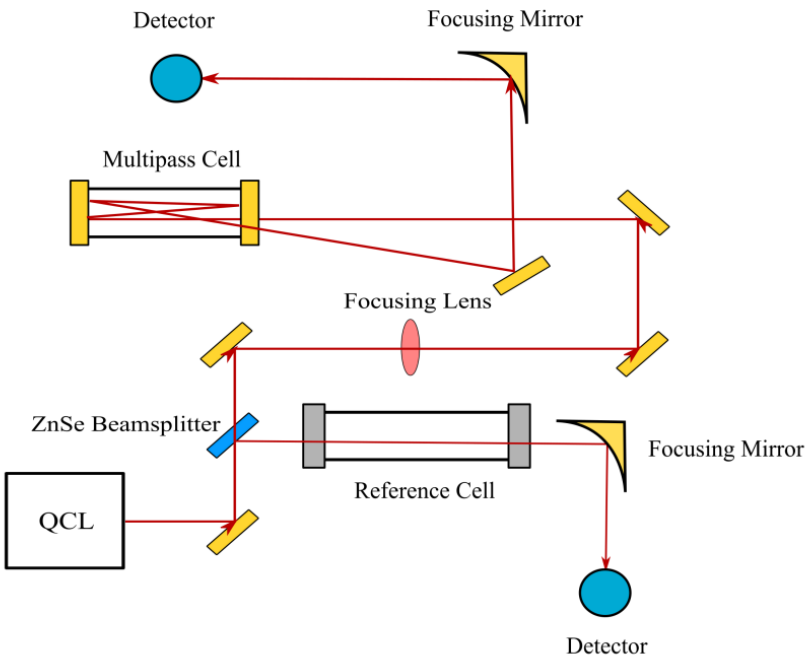

Figure 9. A diagram of QCL-spectrometer setup.

2. Sweep-scan and piezo-scan

Two scanning methods were used to acquire *trans*-1,3-pentadiene spectra. The first method is sweep-scan, in which the light is swept over several wavenumbers using a frequency sweep function built inside the laser controller. The light coming from the light source is directed through each cell and the transmitted intensity is sent to the detectors. Sweep-scan can obtain spectra of a wide frequency range in a few seconds. This feature provides an overall view of the spectra, especially when the pressure of the system cannot be kept consistent for a long time, leading to differences in the relative absorbance from scan to scan. However, sweep-scan has certain limitations for high-resolution spectroscopy. A mechanical motor is used to turn the angle of diffraction grating inside the laser, which changes the frequency emitted so the angle change can determine the smallest step size of the laser. Also, when using sweep-scan, the laser is prone to

mode hops, especially at the edges of the frequency range. The transmittance peaks can be distorted and have irregular shapes, leading to inaccuracy in calibration.

The second type of scanning, piezo-scan, can help to alleviate these problems. The piezo which is made of PZT material, is built inside the laser. Applied voltage can change the width of the piezo electric materials, which can control the positions of the optics inside the laser. By changing the width of PZT materials, the optical components can be moved precisely, emitting radiation of more accurate frequencies. Piezo-scan also involves a function generator (Siglent, SDG1025) and a piezo controller (ThorLabs, MDT694B). The piezo controller scans a small range of wavenumber back and forth with a sine function created by the function generator. The parameters in the function generator are 3 Hz (frequency), 10 Vpp (amplitude) and 5 Vdc (offset). As the piezo controller scans the same region multiple times, piezo-scan increases the number of averages and improves signal-to-noise ratio, providing higher resolution spectra than sweep-scan. Piezo-scanning is smoother so it does not lead to distorted peaks and lineshapes, which are observed frequently in sweep-scan. While piezo-scan can provide higher resolution, it can only scan a small range of wavenumber (0.7-0.8 cm^{-1}) per scan so multiple scans are combined to obtain a wide-range spectrum, which is not desirable for a system with leaks or fluctuating pressure.

As sweep-scan and piezo-scan complement each other, both types were used to obtain high-resolution spectra of *trans*-1,3-pentadiene.

3. Sample preparation

A mixing station was created to prepare samples of *trans*-1,3-pentadiene. A valve system (Nupro Company, SS-4H-TH3) is connected to a vacuum pump (Varian, NW-25), a pressure gauge (MKS Instruments, 626C13TBE), a nitrogen tank, a 250 mL- glass bulb (Chemglass Airfree) and a

bubbler. The nitrogen tank is connected to the mixing station by Teflon tubing while the other connections are made with plastic tubing.

Trans-1,3-pentadiene was obtained from TCI Chemicals (>93.0% purity). A few drops were added to the bubbler and the compound was degassed using two freeze-pump-thaw cycles with liquid nitrogen. When *trans*-1,3-pentadiene was frozen, all impurity gases were pumped out. After the system was evacuated and the pressure was under 0.020 torr, *trans*-1,3-pentadiene was introduced to the system. The pressure was kept below 1 torr to avoid saturated absorbance peaks. The glass bulb containing *trans*-1,3-pentadiene was removed and transferred to the system connected to the multipass cell for absorbance measurement.

4. Sample measurements

Trans-1,3-pentadiene was added to the multipass cell and the pressure was kept below 0.5 torr to avoid saturation. The low pressure also decreases the linewidths of individual rotational lines, which allows us to acquire the high-resolution spectrum. At higher pressures, the peaks become broader and start to blend together so the fine structure in the spectrum cannot be observed. Multiple piezo-scans were taken continuously in the range of 970-1017cm^{-1}. As the piezo controller only scans 0.7-0.8 cm^{-1} per scan and the scans can overlap, each scan was taken 0.5 cm^{-1} apart to avoid gaps.

After all piezo-scans were taken, the system was evacuated and flushed with nitrogen three times to remove *trans*-1,3-pentadiene. The signals indicated the amount of light coming to the detector, or the transmittance, instead of the absorbance. Therefore, a sweep-scanned background spectrum was taken from 970 to 1017 cm^{-1} for absorbance calculation.

For all scans, *trans*-1,3-pentadiene (or nitrogen) in the multipass cell and methanol in the reference cell were scanned simultaneously for frequency calibration.

5. Calibration

The acquired methanol spectra were compared with a reference methanol spectrum in the region of 970-1017 cm^{-1} generated by SpectraPlot and the HITRAN database.[21, 22] The parameters were chosen to be similar to the conditions inside the reference cell: P= 0.001 atm, T= 300 K and L= 50 cm. An example of an acquired methanol spectrum and its corresponding region in the methanol spectrum generated by Spectraplot using the HITRAN database is provided in Figure 10.[21, 22]

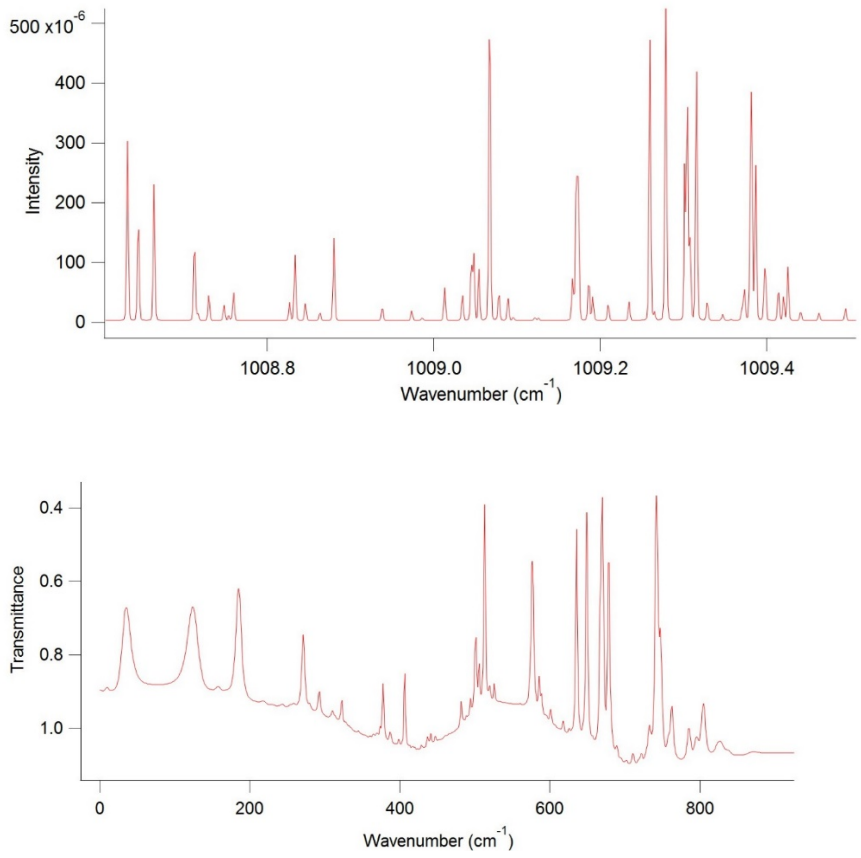

Figure 10. An acquired methanol spectrum and its corresponding region of 1008.6- 1009.4 cm^{-1} in the methanol spectrum generated by SpectraPlot and the HITRAN Database. [21, 22]

The peaks in the acquired spectra were matched with the corresponding peaks in the reference spectrum. A 10^{th}-order polynomial curve was fitted with x and y values as point number in the acquired spectrum and reference wavenumber respectively. The fitting curve can calculate the frequency of each point in the acquired spectra. As all scans were taken for both methanol and *trans*-1,3-pentadiene simultaneously, the calibrated wavenumbers in the methanol spectra were the same in the sample spectra. All acquired background and sample spectra were calibrated using this method with a program written in the Igor Pro software package (Wavemetrics). The absorbance spectra were obtained using the background and sample spectra's transmittance.

6. Theoretical Calculations

The molecular structure of *trans*-1,3-pentadiene was calculated at the MP2/cc-pVTZ level of theory using the GAUSSIAN 16 software.[23] Anharmonic vibrational frequencies and rotational constants were calculated using second-order vibrational perturbation theory.[24] The calibrated frequencies were compared to calculated anharmonic vibrational frequencies and observed values in the study by Compton and George.[6]

The rotational constants of the ground state were obtained from the study by Hsu and Flygare; the rotational constants of the first excited vibrational state were calculated.[7] With the rotational constants of ground and first-excited vibrational state, a theoretical spectrum of *trans*-1,3-pentadiene was simulated by PGOPHER,[25] which was then compared with the acquired spectrum.

Results and Discussion

1. High-resolution absorbance spectrum of trans-1,3-pentadiene

a. Piezo-scanned spectra of *trans*-1,3-pentadiene

Piezo-scanned spectra of *trans*-1,3-pentadiene were taken continuously from 970 to 1017 cm^{-1}. As it is difficult to transfer the same amount of *trans*-1,3-pentadiene to the multipass cell every time, acquiring spectra at the same settings can minimize the difference in the relative absorbance values from scan to scan. All piezo-scanned spectra were calibrated and combined into a single spectrum in the region of 970-1017 cm^{-1}. Spectra were colored as red and orange to distinguish the different spectra next to each other (Figure 11).

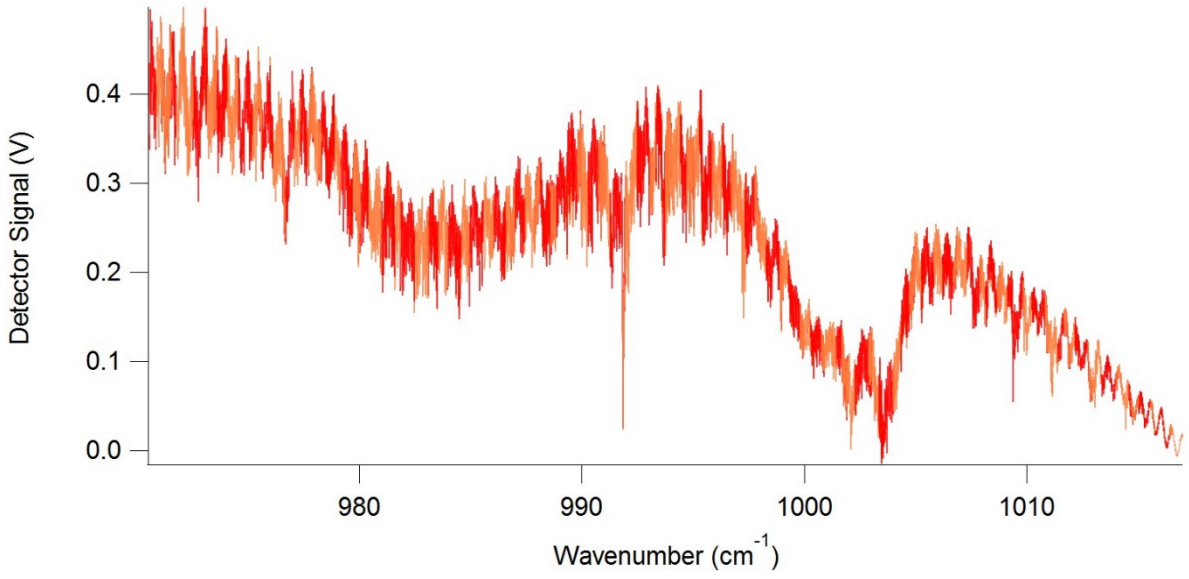

Figure 11. Multiple calibrated spectra combined into a single spectrum of *trans*-1,3-pentadiene in the region of 970-1017 cm^{-1}.

Overlapping spectra were examined to estimate the uncertainty in the calibrated frequency. The frequency uncertainty, estimated as the average difference of frequencies in two overlapping scans, is 0.002 cm^{-1}. The difference in calibrated frequency of any two spectra next to each other was inconsistent. While some spectra lined up very well in which the difference in calibrated frequency was less than 0.001 cm^{-1}, there were others with bigger deviation (0.002 cm^{-1}) (Figure 12).

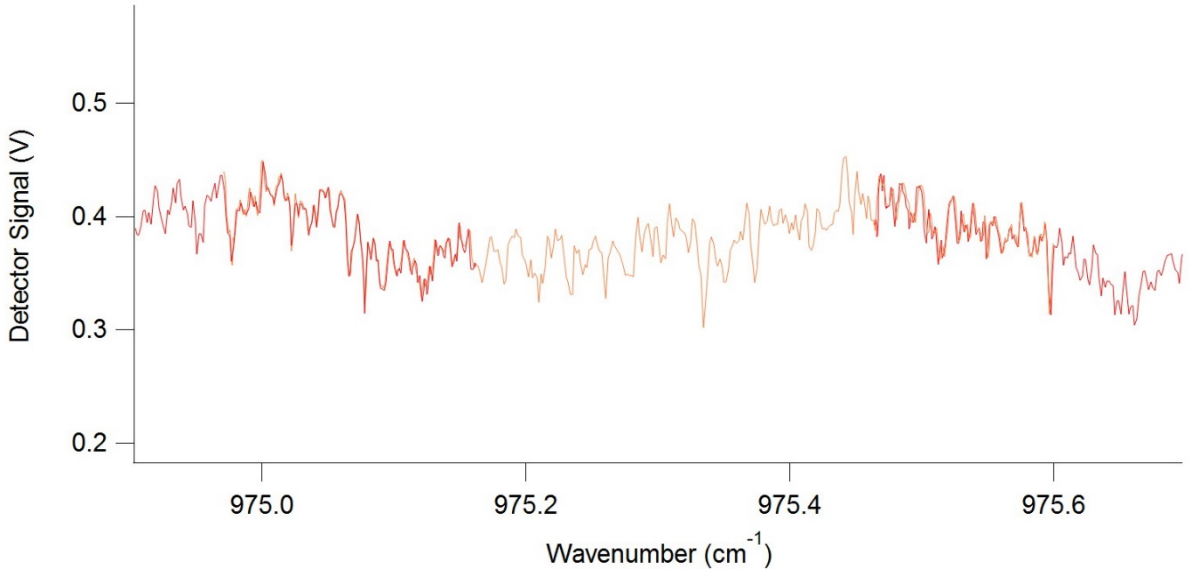

Figure 12. The difference in wavenumber of two overlapping spectra might vary from 0.0005 to 0.002 cm^{-1}. The overlapping region of 974.97- 975.16 cm^{-1} had the average deviation of 0.0008 cm^{-1} while the overlapping region of 975.46-975.60 had the average deviation of 0.002 cm^{-1}.

Some of the uncertainty in the calibration comes from the methanol reference spectrum as the frequencies obtained from the HITRAN Database also have uncertainty. The parameters (temperature or pressure) in this laboratory setting could be different from the values used to compute the SpectraPlot reference spectrum. As a result, there might be a small deviation between our spectrum and the SpectraPlot spectrum.

Another source of uncertainty comes from methanol signals. Methanol absorbs strongly at certain regions while there are fewer peaks in other frequencies (Figure 13). If there are less points to calibrate, the fitting curve is less exact, leading to higher uncertainty. For example, in the range of 970-980 cm^{-1}, the peaks are relatively weak, which makes it difficult to distinguish these peaks from the change in the background. When the peaks overlap and become a broad single peak, they cannot be separated and assigned to the corresponding peaks in the reference spectrum. Even in the range of 990-1010 cm^{-1} where methanol absorbs strongly, the number of peaks are not even for all frequencies. The scans with more peaks calibrated are more exact than the scans with fewer peaks. Therefore, the difference in calibrated wavenumbers of any two spectra next to each other was inconsistent.

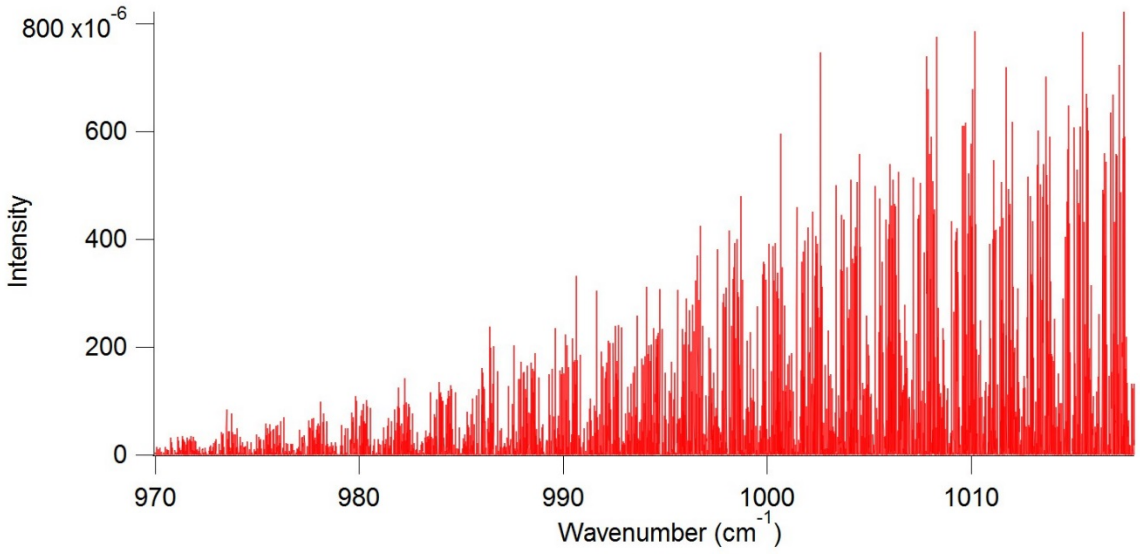

Figure 13. Methanol reference spectrum in the region of 970-1017 cm^{-1} generated by SpectraPlot based on the HITRAN database.[21, 22]

Despite this disadvantage, methanol was still used for calibration because it has many more absorption peaks in the infrared range of 970-1017 cm^{-1} compared to other compounds reported in

the HITRAN database. Methanol is cheap and it is liquid in room temperature so it is easy to transfer the compound to the system. Methanol also has strong absorption peaks, which makes the calibration simpler.

b. Sweep-scanned background spectrum

Absorbance is defined as the capacity of a substance to absorb radiation of a specific wavelength. It is calculated using the following equation:

$$\text{Absorbance} = -\log\frac{I}{I_0}$$

in which I and I_0 are the sample and background signal respectively.

To determine absorbance, the background signal is required so a single spectrum of background was acquired by sweep-scan after *trans*-1,3-pentadiene was pumped out from the system (Figure 14). The background spectrum was calibrated using the methanol reference spectrum as above.

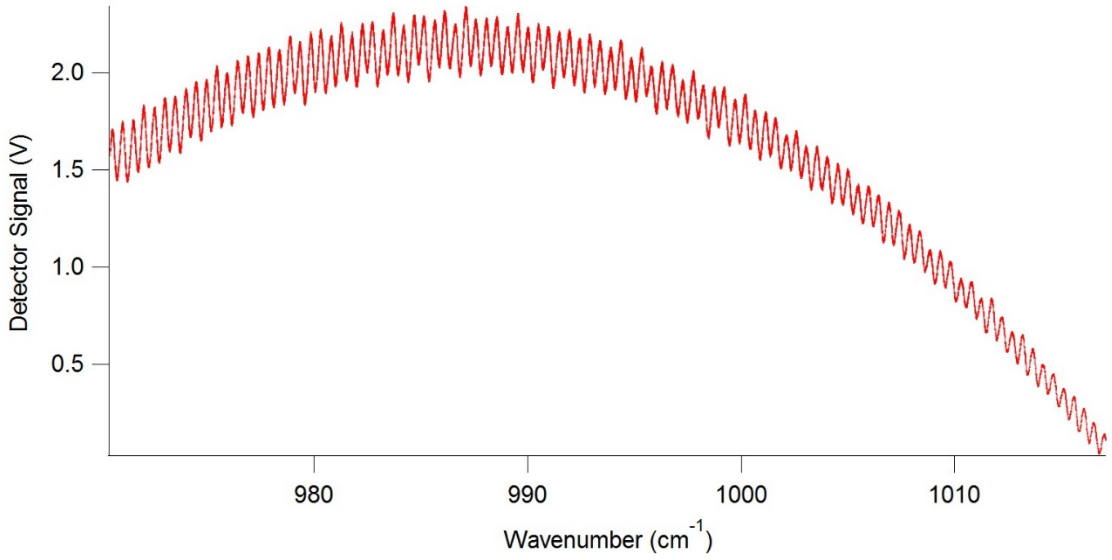

Figure 14. Calibrated background spectrum in the region of 970-1017 cm^{-1} acquired by sweep-scan.

c. High-resolution absorbance spectrum of *trans*-1,3-pentadiene

A program was written in Igor Pro software package based on the interpolate function, which simply finds the detector signal for an intermediate value of the frequencies. The absorbance of *trans*-1,3-pentadiene was calculated using the above equation. A single absorbance spectrum of *trans*-1,3-pentadiene in the region of 970-1017 cm^{-1} was obtained (Figure 15). Major peaks observed in this region included: 976.69 (weak), 991.87 (strong), 1002.10 (strong), 1003.50 (very strong), 1009.42 (weak), 1011.18 (weak), 1012.98 (weak) and 1014.68 (weak) cm^{-1} (Figure 16).

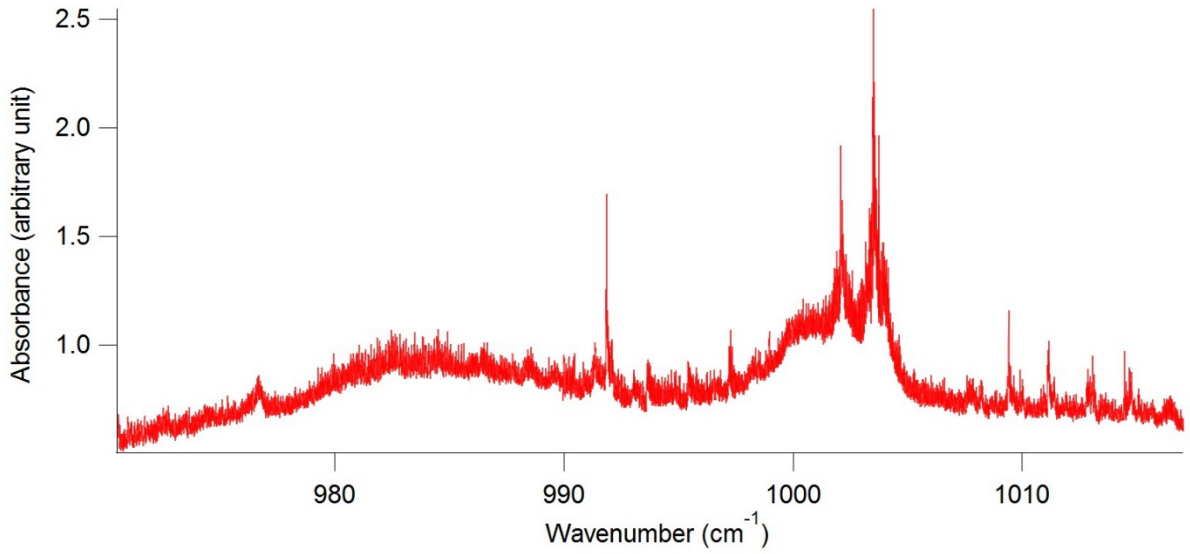

Figure 15. High-resolution absorbance spectrum of *trans*-1,3-pentadiene in the calibrated region of 970 to 1017 cm^{-1}

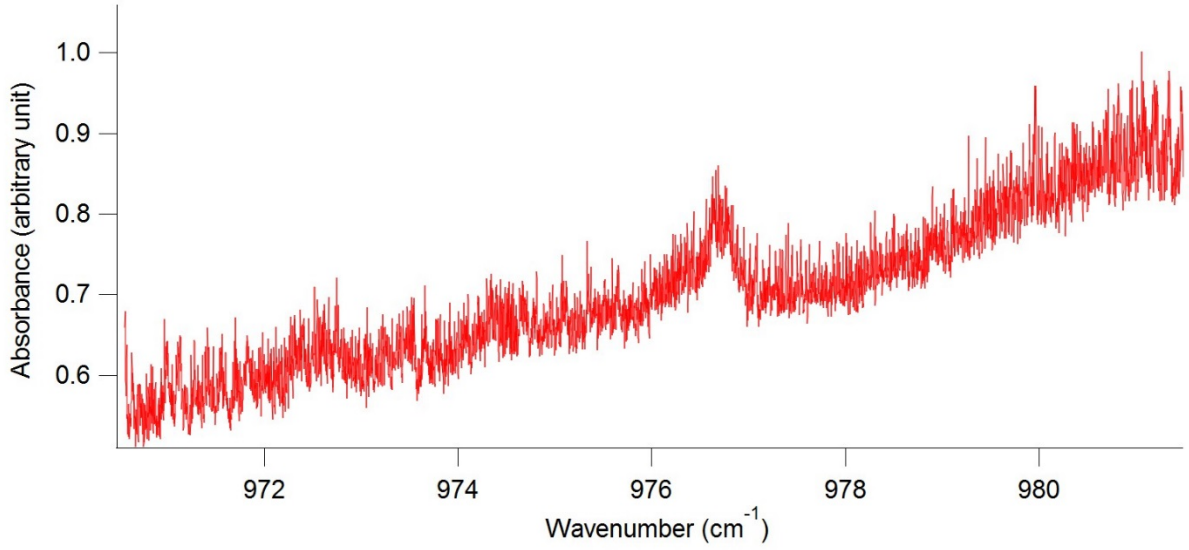
Absorbance (arbitrary unit)
1.0
0.9
0.8
0.7
0.6
972
974
976
978
980
Wavenumber (cm-1)

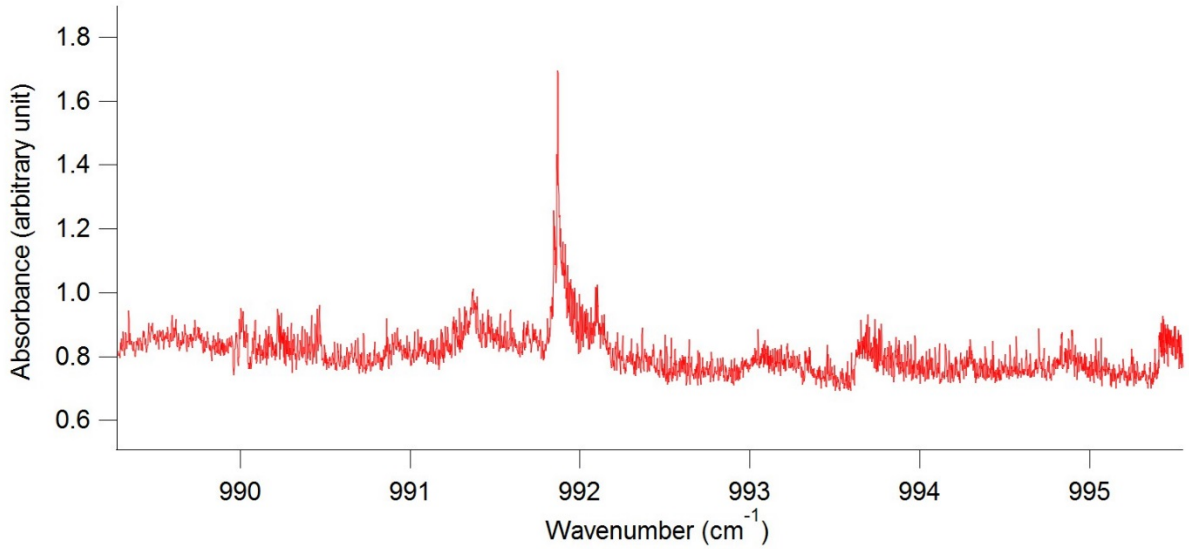
Absorbance (arbitrary unit)
1.8
1.6
1.4
1.2
1.0
0.8
0.6
990
991
992
993
994
995
Wavenumber (cm-1)

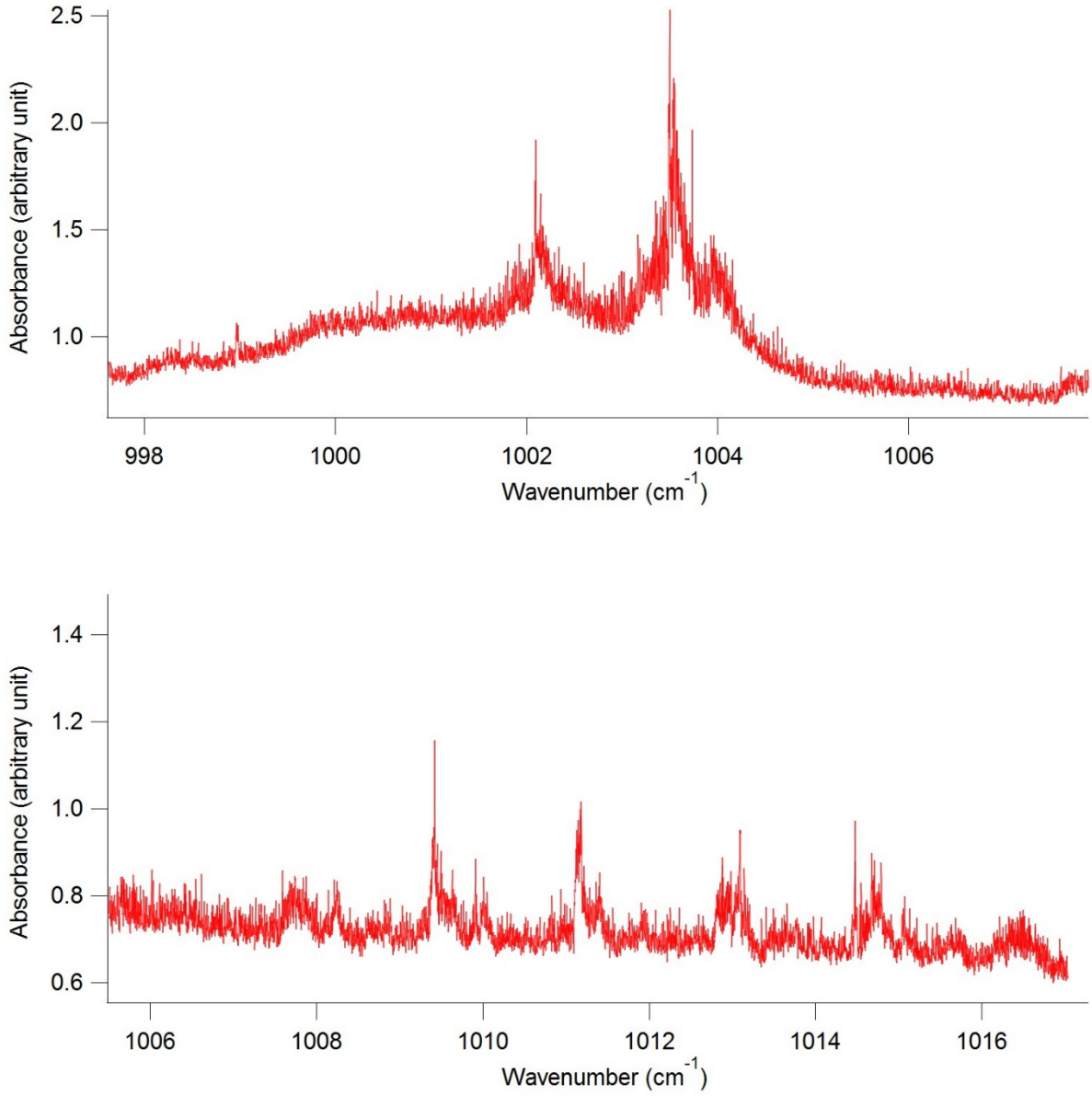

Figure 16. Zoom-in spectrum in the region of major peaks at 976.69, 991.87, 1002.10, 1003.50, 1009.42, 1011.18, 1012.98 and 1014.68 cm^{-1}.

In the study by Compton and George, *trans*-1,3-pentadiene was reported to have two peaks at 977 (weak) and 1003.3 (very strong) cm^{-1}, which were also observed at slightly different frequency in our spectrum (976.69 and 1003.50 cm^{-1}).[6] Four weak peaks at 1009.42, 1011.18, 1012.88 and 1014.68 cm^{-1} were reported as satellite bands in this paper. A plot of nine satellite peaks between

1005 and 1020 cm^{-1} gave a straight line of slope 1.73 cm^{-1}.[6] Four observed peaks were fitted into a linear equation and obtained a slope of 1.748 cm^{-1}. For a prolate top, satellite bands should be observed with a spacing of 2(A-B), which is 1.74 cm^{-1} for *trans*-1,3-pentadiene.[7] The observed value is within 0.5% error of the theoretical value, which indicates that treating the molecule as a near prolate top is a good approximation.

The peak at 991.87 cm^{-1} was assigned to the Q-branch of the ν_{26} vibrational band of isoprene, which is another compound studied in this laboratory setup. As it was almost impossible to remove all isoprene from the mixing station, there was always a small amount of isoprene transferred to the multipass cell along with *trans*-1,3-pentadiene. However, this peak does not overlap with any vibrational mode of *trans*-1,3-pentadiene so it does not affect the analysis.

Other weaker peaks were also observed in the range of 970-1000 cm^{-1}. It is difficult to identify the broad peaks so the calibrated spectrum was compared with the theoretical spectrum simulated by PGOPHER to match peaks of the same frequencies.

2. Theoretical calculations

The molecular structure of *trans*-1,3-pentadiene was calculated at the MP2/cc-pVTZ level of theory using the GAUSSIAN 16 software.[23] Vibrational motion in a molecule can be approximated as a harmonic oscillator and anharmonic parts account for the deviation of the system from the simple harmonic motion. As *trans*-1,3-pentadiene is not a diatomic molecule, anharmonicity is important in defining the vibrational spectrum. Anharmonic vibrational frequencies were calculated using second-order vibrational perturbation theory.[24] Using the rule 3N-6 vibrational modes (where N is the number of atoms in the molecule), *trans*-1,3-pentadiene has 33 vibrational modes. As the sample was examined at room temperature, fundamental transitions were dominant.

Overtones and combination bands calculated by the program were also examined but none of the transitions occurs near the region of 970-1017 cm^{-1}. Calculated fundamental anharmonic vibrational frequencies and their relative intensities are presented in Table 1.

There are two vibrational frequencies in the region of 970-1017 cm^{-1}: 979 and 1021 cm^{-1}, which can be matched up with the peaks at 976.69 and 1003.50 cm^{-1} in our calibrated spectrum respectively. The band at 1021 cm^{-1} has the strongest intensity (40.7), which corresponds well to the relative intensity of the strongest observed peak at 1003.5 cm^{-1} (Table 1). The observed peak at 976.69 cm^{-1} was a weak peak and the calculated band at 979 cm^{-1} has relative intensity of 7.75, which equals to approximately one fifth of the strongest band at 1021 cm^{-1} (Table 1). Anharmonic vibrational frequencies are often higher than the observed values and *trans*-1,3-pentadiene is a fairly large molecule for an *ab initio* calculation so agreement within 20 cm^{-1} is reasonable.

Table 1. Anharmonic vibrational frequencies and their intensities calculated by GAUSSIAN 16 software.[23] Red values correspond to the two observed vibrational bands in the calibrated spectrum.

Mode(n)	E(cm^{-1})	Intensity (km/mol)
1(1)	3144	10.5
2(1)	3032	0.0
3(1)	2996	8.4
4(1)	3065	2.6
5(1)	3043	0.9
6(1)	3015	5.4
7(1)	2966	12.0
8(1)	1673	8.5
9(1)	1616	3.0
10(1)	1467	7.3

11(1)	1421	4.0
12(1)	1382	2.3
13(1)	1308	2.6
14(1)	1296	0.0
15(1)	1268	0.2
16(1)	1191	0.7
17(1)	1092	0.0
18(1)	979	7.8
19(1)	825	4.8
20(1)	638	1.9
21(1)	480	0.0
22(1)	449	0.3
23(1)	2996	14.9
24(1)	1450	4.8
25(1)	1041	0.3
26(1)	1022	40.7
27(1)	960	9.4
28(1)	908	34.0
29(1)	905	4.0
30(1)	255	2.1
31(1)	283	1.2
32(1)	196	1.5
33(1)	47	0.2

In the study by Compton and George, all 33 vibration modes were reported with frequencies and description of motions.[6] By convention, the vibration modes were assigned from number 1 to 33 in the order of decreasing wavenumbers. In-plane vibrations are assigned a number before out-of-plane vibrations (Table 2).

Table 2. 33 normal modes of *trans*-1,3-pentadiene were reported with frequencies and descriptions of motions.

ν	Experimental frequency (cm^{-1})	Vibration	In-plane (A')/ Out-of-plane (A")
1	3098	asym =C-H stretch	A'
2	3050	asym -CH= stretch	A'
3	3018	sym -CH= stretch	A'
4	2997	sym =C-H stretch	A'
5	2980	sym =C-H stretch	A'
6	2973	asym methyl C-H stretch	A'
7	2931	sym methyl C-H stretch	A'
8	1660	C=C sym-stretch	A'
9	1608	C=C asym-stretch	A'
10	1449	Methyl asym-deformation	A'
11	1420	=CH2 scissor	A'
12	1376	Methyl sym-deformation	A'
13	1306	-CH= bend	A'
14	1280	-CH= bend	A'
15	1180	Methyl rock	A'
16	1170	=C-C= stretch	A'
17	1082	C-CH3 stretch	A'
18	977	=CH2 rock	A'
19	630	Skeletal mode	A'
20	483	Skeletal mode	A'
21	454	Skeletal mode	A'
22	383	Skeletal mode	A'
23	2946	Methyl C-H Stretch	A"
24	1435	Methyl deformation	A"
25	1048	Methyl rock	A"

26	1003.3	*trans*-CH=CH wag	A"
27	948.5	*trans*-CH=CH wag	A"
28	899	=CH2 wag	A"
29	698	*cis*-CH=CH wag	A"
30	250	Skeletal mode	A"
31	205	Methyl torsion	A"
32	196	Skeletal mode	A"
33	150	=C-C= torsion	A"

The two peaks observed at 976.69 and 1003.50 cm^{-1} correspond to the peaks at 977 and 1003.3 cm^{-1} in this paper and were assigned to ν_{18} and ν_{26} bands respectively. Based on this paper, the two peaks at 977 and 1003.3 cm^{-1} were also assigned to $=CH_2$ rock and *trans*-CH=CH wag. The vibration modes calculated by the GAUSSIAN 16 software showed the motion of the molecule (Figure 17, 18).

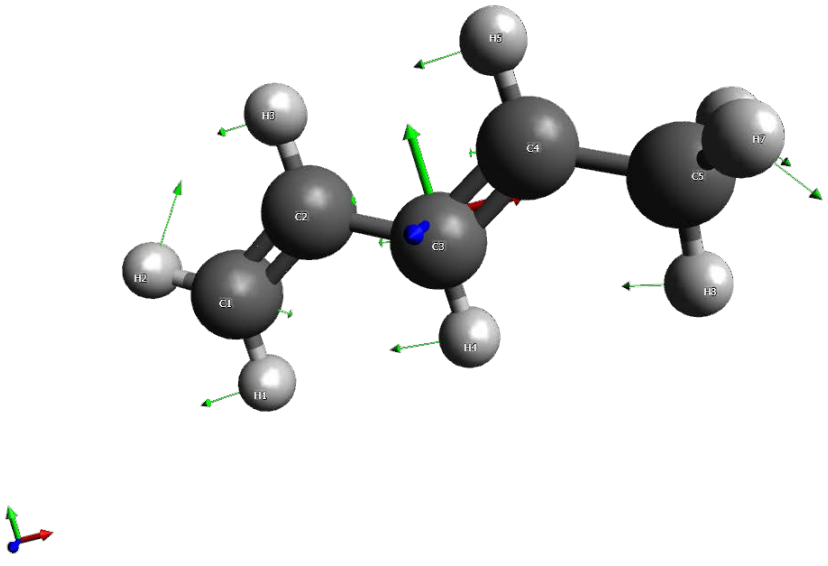

Figure 17. The motion of =CH2 rock corresponds to the vibration mode ν_{18}

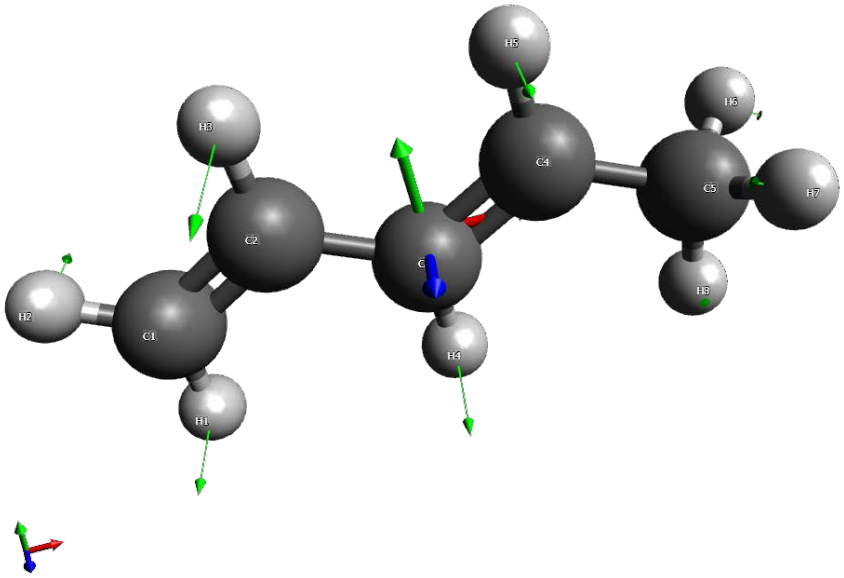

Figure 18. The motions of trans CH=CH wag corresponds to ν_{26}

3. Simulated vibrational spectrum of trans-1,3-pentadiene

A ro-vibrational spectrum of *trans*-1,3-pentadiene was simulated by PGOPHER to assign peaks of ν_{26} band to specific transitions.[25] The rotational constants for the ground and first excited state were calculated using second-order vibrational perturbation theory.[24] The experimental values of rotational constants for the ground state of *trans*-1,3-pentadiene was obtained from a paper by Hsu and Flygare.[7] Assuming that the difference in the rotational constants of the ground and first excited state is the same for both calculated and experimental values, adjusted rotational constants of the first excited state were calculated using the following equation:

$$A'_{\text{adjusted}} = A''_{\text{experimental}} + (A'_{\text{calculated}} - A''_{\text{calculated}})$$

in which A' and A'' stands for rotational constants of ground and first excited state respectively.

Rotational constants values used for the simulated vibrational spectrum of ν_{26} transition are presented in Table 3.

Table 3. Rotational constants of the ground state and the first excited state of ν_{26}.

	A (MHz)	B (MHz)	C (MHz)
Ground state	28200	2160.61	2033.21
First-excited state of ν_{26}	28150	2162.59	2033.63

The simulated ro-vibrational spectrum of *trans*-1,3-pentadiene was compared with the calibrated spectrum in the region of 970-1017 cm^{-1} (Figure 19).

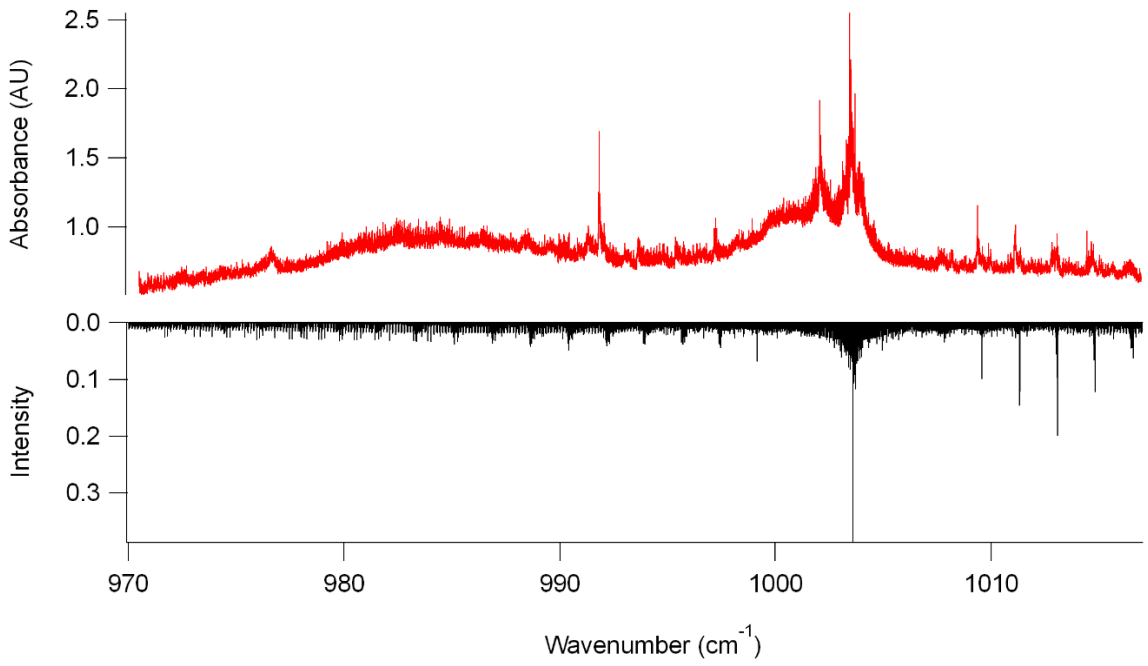

Figure 19. Simulated vibrational spectrum (black) and calibrated vibrational spectrum (red) of *trans*-1,3-pentadiene in the region of 970-1017 cm^{-1}.

Major peaks in the calibrated spectrum were observed in the simulated spectrum: 1003.50 (very strong), 1009.42 (weak), 1011.18 (weak), 1013.10 (weak) and 1014.48 (weak) cm^{-1} except the peak at 1002.10 cm^{-1} (Figure 20, 21).

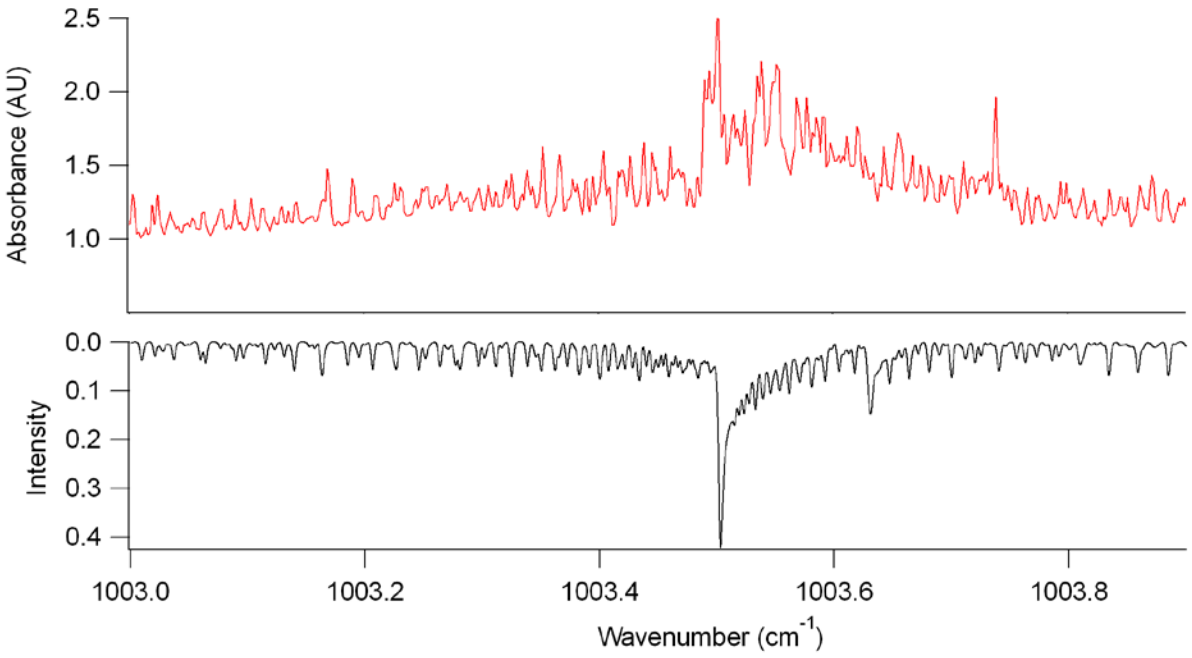

Figure 20. Strong peak at 1003.5 cm^{-1} was assigned to ν_{26} vibrational band of *trans*-1,3-pentadiene

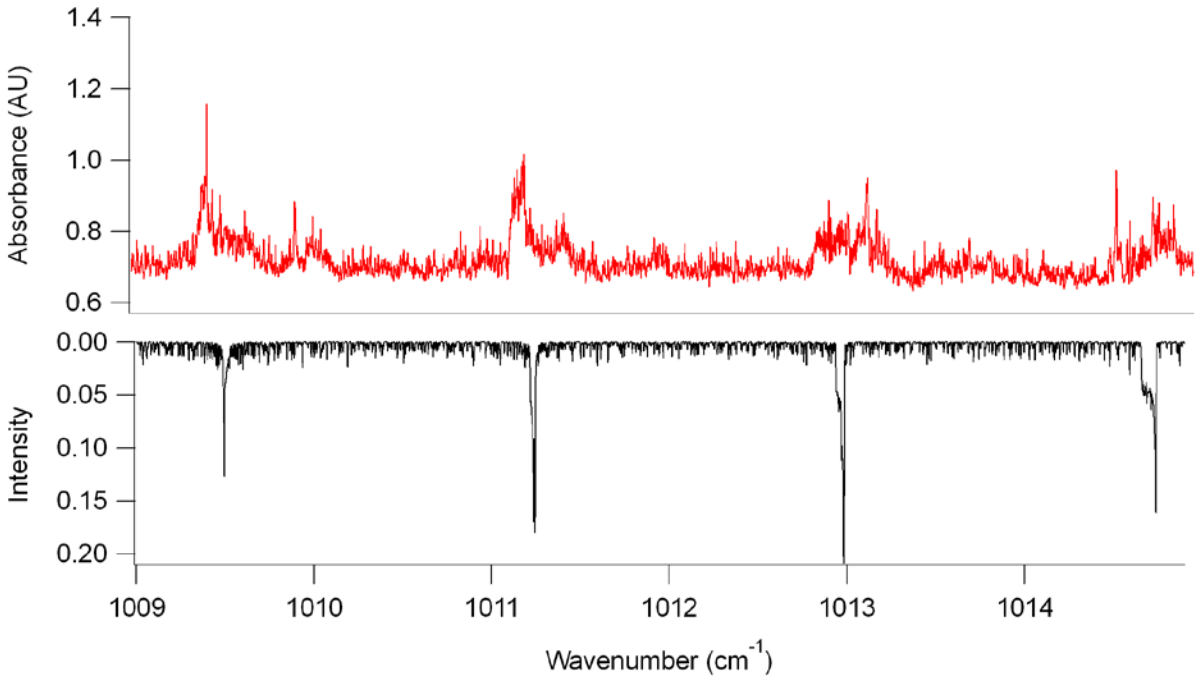

Figure 21. Four weak peaks at 1009.42 (weak), 1011.18 (weak), 1013.10 (weak) and 1014.48 (weak) cm^{-1} were assigned to satellite bands of ν_{26}.

Some weak peaks in the calibrated spectrum which were difficult to distinguish from weaker rotational lines were also matched with peaks of the same wavenumbers in the simulated spectrum. Those include weak peaks at 993.69, 995.43, 997.28 and 998.97 cm^{-1} in the calibrated spectrum (Figure 22). The weak peak at 992.14 cm^{-1} lies close to the Q-branch peak of isoprene at 992.09 cm^{-1} (Figure 23).

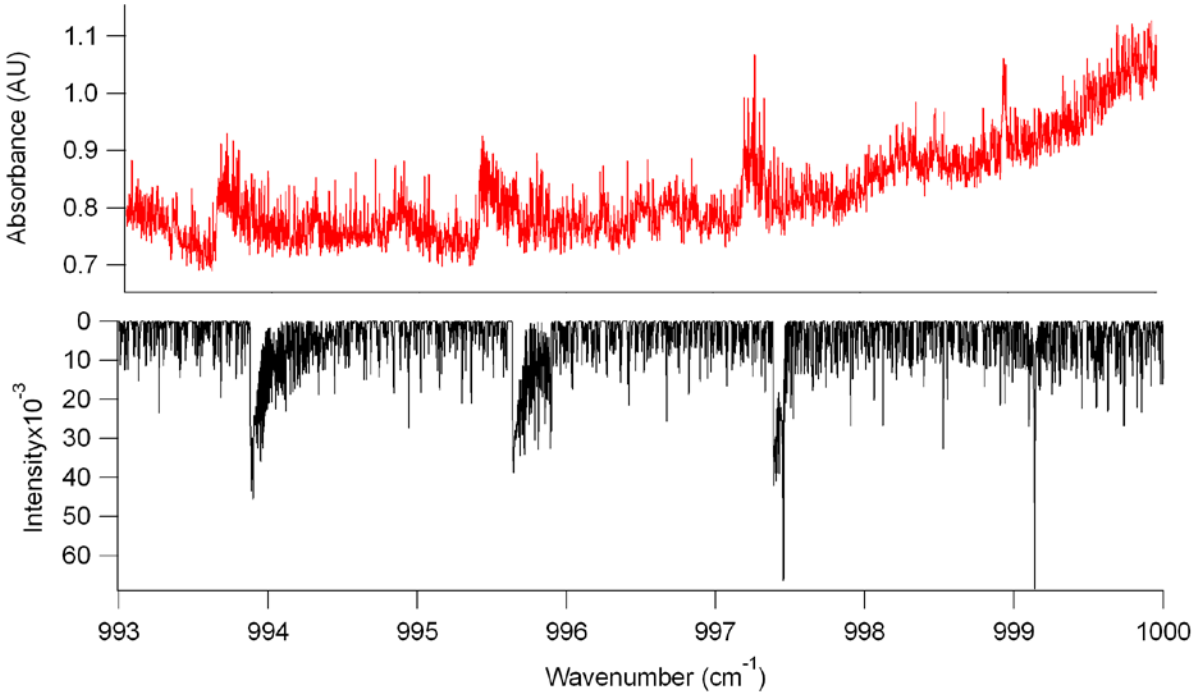

Figure 22. Four weak peaks at 993.69, 995.43, 997.28 and 998.97 cm^{-1} were identified using the simulated spectrum.

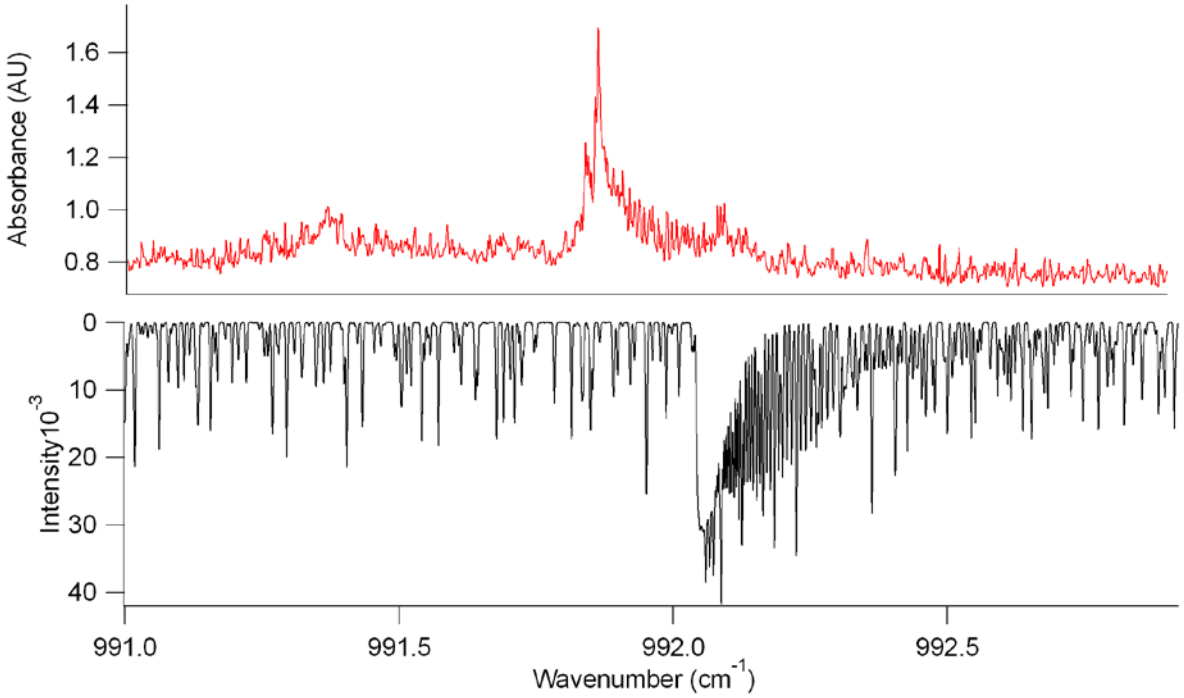

Figure 23. A weak peak at 992.14 cm^{-1} is close to a Q-branch peak of isoprene at 992.09 cm^{-1}

Multiple peaks in the range of 984-991 cm^{-1} of the simulated spectrum were also observed in the calibrated spectrum as very broad peaks. Without the simulated spectrum, it was difficult to identify those peaks. Those peaks are centered at: 984.94, 986.67, 988.57 and 990.22 cm^{-1} (Figure 24).

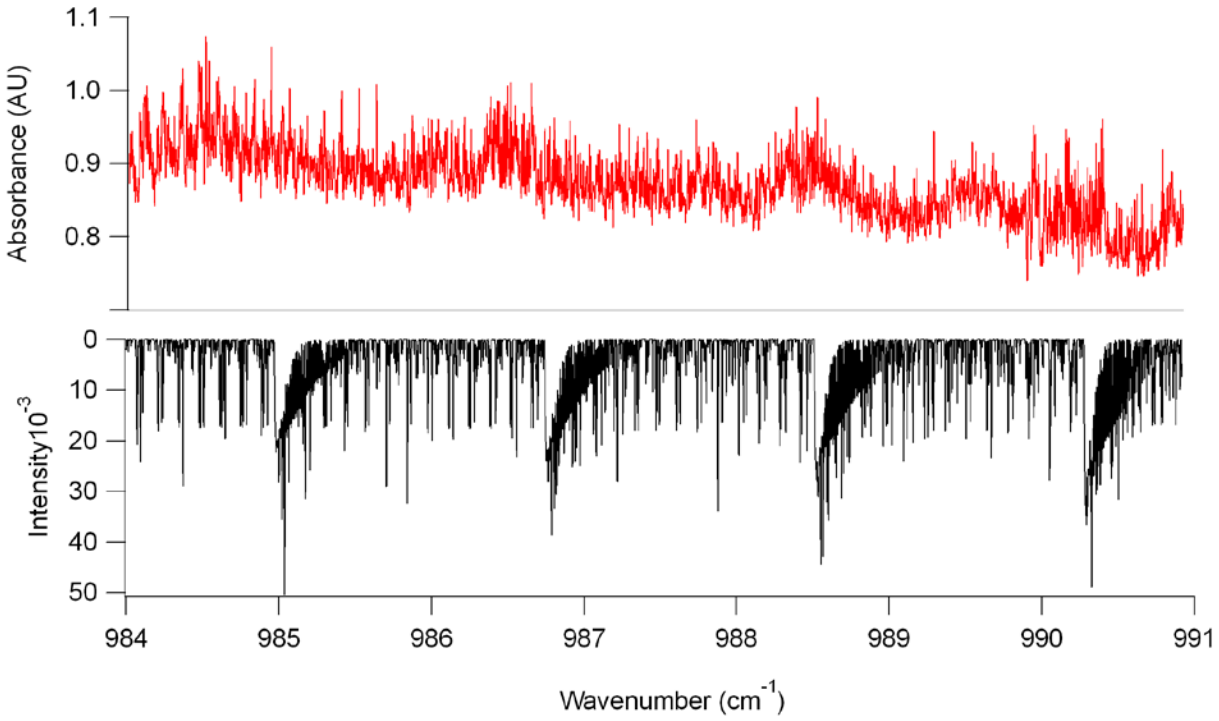

Figure 24. Four weak peaks at 984.94, 986.67, 988.57 and 990.22 cm^{-1} were identified using the simulated spectrum.

Multiple peaks in the range of 970-984 cm^{-1} of the simulated spectrum were unidentified in the calibrated spectrum as they were too weak to be distinguished from other rotational lines (Figure 25). An explanation for the relatively low intensities of these observed peaks is that the actual rotational constants are slightly off from the computed rotational constants, so the peaks are much weaker than predicted.

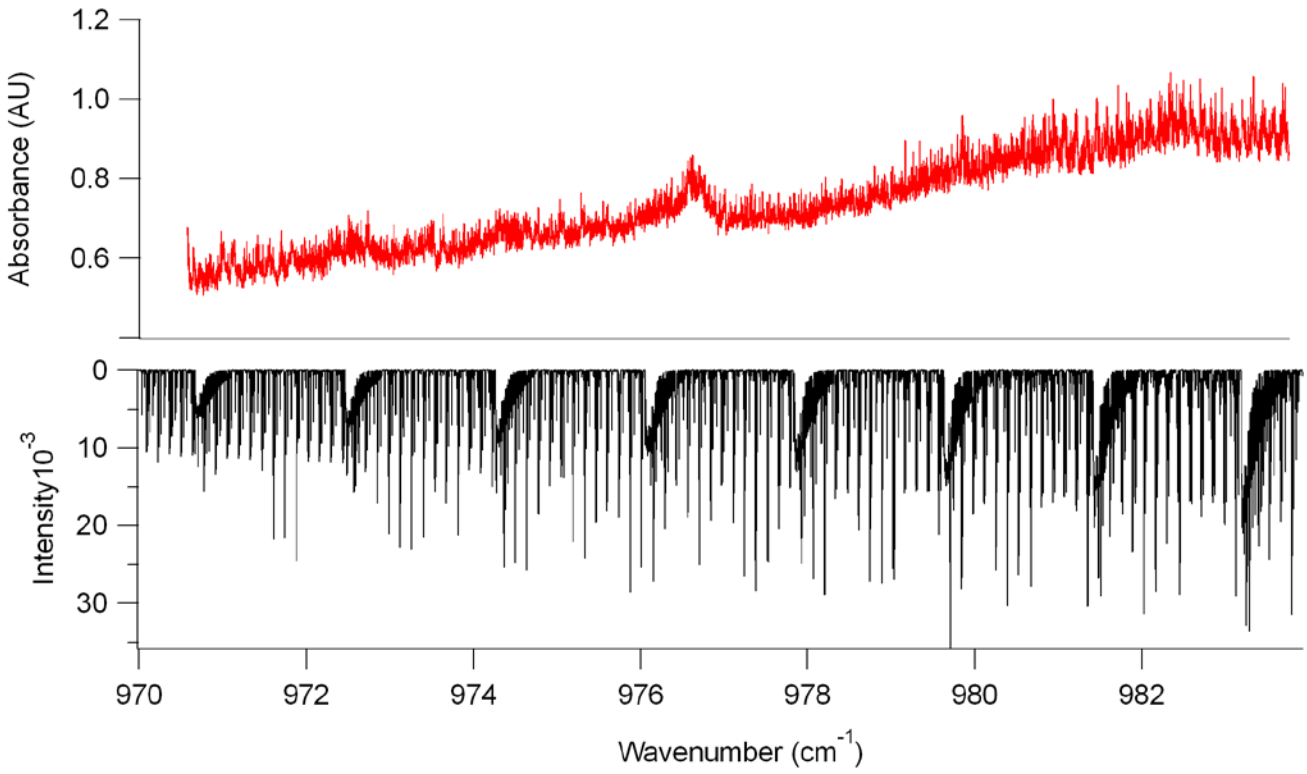

Figure 25. Multiple unidentified peaks in the region of 970- 984 cm^{-1}.

The strong observed peak at 1002.10 cm^{-1} was not present in the simulated spectrum. While calculated frequencies of overtones and combination bands showed no band at this wavenumber, it is common to observe a hot band in the Q-branch. This peak was assigned to the hot band of ν_{26} transition due to their similar shapes (Figure 26). A hot band refers to the transition in which molecules in excited states absorb infrared radiation and jump to a higher excited state. Because *trans*-1,3-pentadiene has anharmonic terms in its vibrational energy equation, the energy levels are not equally spaced as in the harmonic oscillator and the energy gap becomes closer with increasing v. As a result, the energy gap between two states in a hot band transition is smaller than the value in a fundamental transition. It is reasonable to observe a hot band at lower frequency (1002.10 cm^{-1}) than the fundamental transition (1003.50 cm^{-1}).

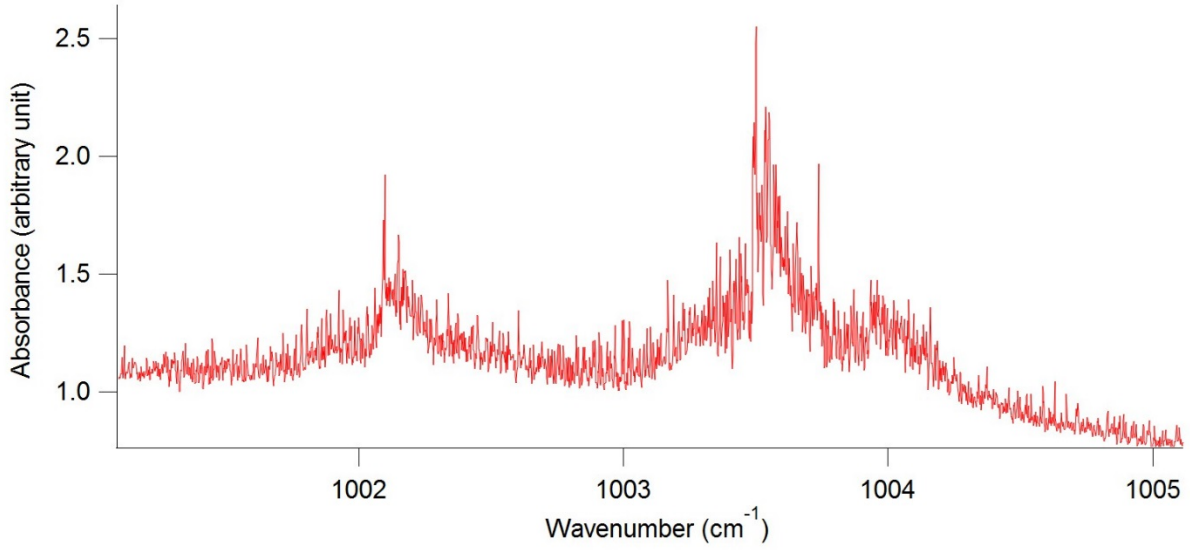

Figure 26. The peak at 1002.10 cm^{-1} was assigned to the hot band of ν_{26} due to its relatively strong intensity and similar shape to this vibrational mode.

In addition, the relatively strong intensity of the peak at 1002.10 cm^{-1} indicates that the hot band likely comes from the excitation of the molecule in the lowest lying vibrational mode ν_1 (150 cm^{-1}) to ν_{26} (1003.5 cm^{-1}) mode.[6] The Boltzmann factor, which is the ratio of population distribution of two states can also explain the relative intensity of the hot band. The Boltzmann factor associated with ν_1 with respect to the ground state is given in the following equation:

$$\frac{F_1}{F_0} = e^{\frac{E_0 - E_1}{kT}}$$

in which $\frac{F_1}{F_0}$ is the Boltzmann factor, E_0 and E_1 are the energies of the ground state and the lowest vibrational mode in cm^{-1} respectively, T is the temperature in Kelvin, k is the Boltzmann constant and k = 0.695 cm^{-1}/K.

In this lab setting, T was 300 K, E_0 is set to be 0 cm^{-1} and the value of E_1 is obtained from the work by Compton and George, E_1 = 150 cm^{-1}.[6] The calculated Boltzmann factor for ν_1 is 0.49, indicating

there is a relatively high number of molecules in this excited state compared to the ground state. High value of the Boltzmann factor also suggests the presence of a hot band.

4. Peak assignments

As the program PGOPHER provided information about the transitions of all peaks, by matching observed peaks with the corresponding peaks in the simulated spectrum, the peaks were assigned to certain transitions. By convention, the peaks are classified into P, Q and R branches based on the change in the quantum number J. The change in quantum numbers K_a and K_c divides the transitions into three types: a-type, b-type and c-type transition. A single peak can be constituted by multiple transitions, which have similar frequencies. These transitions can have different intensities, which will determine the shape of the peak. While there are many transitions that make up the peaks, PGOPHER only lists 10 strongest transitions. The transitions of a single peak can fall into different branches, but the peak is assigned based on the strongest transitions. The entire vibrational band is a c-type transition which has $\Delta K_a = \pm 1$ ($\pm 3, \pm 5, \ldots$), $\Delta K_c = 0$ ($\pm 2, \pm 4, \ldots$) and $\Delta J = \pm 1, 0$. All following transitions assigned to the peaks are *c*-type transitions, which can be observed from the change in K_a and K_c.

Multiple peaks in the region of 970-984 cm^{-1} are too weak to be identified and assigned transitions. The peak at 976.69 cm^{-1} was assigned to the vibration mode ν_{18}.

All other peaks at higher frequency in the calibrated spectrum belong to Q-branch. Most K_a values are the same for all transitions that belong to a particular peak so these transitions line up right on top of each other, which makes a peak stand out.

The transitions assigned to four weak, broad peaks at 984.94, 986.67, 988.57 and 990.22 cm^{-1} are included in the Table 4.

Table 4. Transitions assigned to four Q-branch peak at 984.94, 986.67, 988.57 and 990.22 cm^{-1}.

Observed frequencies (cm^{-1})	Ground state				Excited state				Branch (P,Q,R)	Intensity in the simulated spectrum
	v	J	K_a	K_c	v	J	K_a	K_c		
984.94	0	40	11	29	1	40	10	31	Q	2.76E-05
	0	40	11	30	1	40	10	30	Q	2.76E-05
	0	41	11	30	1	41	10	32	Q	2.76E-05
	0	41	11	31	1	41	10	31	Q	2.76E-05
	0	39	11	28	1	39	10	30	Q	2.75E-05
	0	39	11	29	1	39	10	29	Q	2.75E-05
	0	42	11	31	1	42	10	33	Q	2.75E-05
	0	42	11	32	1	42	10	32	Q	2.75E-05
	0	38	11	27	1	38	10	29	Q	2.74E-05
	0	38	11	28	1	38	10	28	Q	2.74E-05
986.67	0	40	10	30	1	40	9	32	Q	3.04E-05
	0	40	10	31	1	40	9	31	Q	3.04E-05
	0	39	10	29	1	39	9	31	Q	3.04E-05
	0	39	10	30	1	39	9	30	Q	3.04E-05
	0	41	10	31	1	41	9	33	Q	3.04E-05
	0	41	10	32	1	41	9	32	Q	3.04E-05
	0	38	10	28	1	38	9	30	Q	3.03E-05
	0	38	10	29	1	38	9	29	Q	3.03E-05
	0	42	10	32	1	42	9	34	Q	3.03E-05
	0	42	10	33	1	42	9	33	Q	3.03E-05
988.57	0	39	9	31	1	39	8	31	Q	3.32E-05
	0	39	9	30	1	39	8	32	Q	3.32E-05
	0	40	9	32	1	40	8	32	Q	3.32E-05
	0	40	9	31	1	40	8	33	Q	3.32E-05
	0	38	9	30	1	38	8	30	Q	3.32E-05

	0	38	9	29	1	38	8	31	Q	3.32E-05
	0	41	9	33	1	41	8	33	Q	3.32E-05
	0	41	9	32	1	41	8	34	Q	3.32E-05
	0	37	9	29	1	37	8	29	Q	3.31E-05
	0	37	9	28	1	37	8	30	Q	3.31E-05
990.22	0	39	8	32	1	39	7	32	Q	3.59E-05
	0	39	8	31	1	39	7	33	Q	3.59E-05
	0	38	8	31	1	38	7	31	Q	3.59E-05
	0	38	8	30	1	38	7	32	Q	3.59E-05
	0	40	8	33	1	40	7	33	Q	3.59E-05
	0	40	8	32	1	40	7	34	Q	3.59E-05
	0	37	8	30	1	37	7	31	Q	3.58E-05
	0	37	8	29	1	37	7	31	Q	3.58E-05
	0	41	8	34	1	41	7	34	Q	3.58E-05
	0	41	8	33	1	41	7	35	Q	3.58E-05

The peak at 991.87 is Q-branch ν_{26} vibrational band of isoprene and it overlaps with a weak peak of *trans*-1,3-pentadiene. The transitions were not assigned for the peaks at this wavenumber due to the overlapping.

Four weak peaks at 993.69, 995.43, 997.28 and 998.97 cm^{-1} also belong to Q-branch. Their transitions were assigned in Table 5.

Table 5. Transitions assigned to four Q-branch peak at 993.69, 995.43, 997.28 and 998.97 cm^{-1}

Observed frequencies (cm^{-1})	Ground state				Excited state				Branch (P, Q, R)	Intensity in the simulated spectrum
	v	J	K_a	K_c	v	J	K_a	K_c		
993.69	0	38	6	33	1	38	5	33	Q	4.05E-05
	0	38	6	32	1	38	5	34	Q	4.05E-05
	0	37	6	32	1	37	5	32	Q	4.05E-05
	0	37	6	31	1	37	5	33	Q	4.05E-05
	0	39	6	34	1	39	5	34	Q	4.05E-05
	0	39	6	33	1	39	5	35	Q	4.05E-05
	0	36	6	31	1	36	5	31	Q	4.04E-05
	0	36	6	30	1	36	5	32	Q	4.04E-05
	0	40	6	35	1	40	5	35	Q	4.04E-05
	0	40	6	34	1	40	5	36	Q	4.04E-05
995.43	0	37	5	33	1	37	4	33	Q	4.21E-05
	0	37	5	32	1	37	4	34	Q	4.21E-05
	0	36	5	32	1	36	4	32	Q	4.20E-05
	0	36	5	31	1	36	4	33	Q	4.20E-05
	0	38	5	34	1	38	4	34	Q	4.20E-05
	0	38	5	33	1	38	4	35	Q	4.20E-05
	0	35	5	31	1	35	4	31	Q	4.20E-05
	0	35	5	30	1	35	4	32	Q	4.19E-05
	0	39	5	35	1	39	4	35	Q	4.19E-05
	0	39	5	34	1	39	4	36	Q	4.19E-05
997.28	0	31	4	27	1	31	3	29	Q	4.18E-05
	0	30	4	26	1	30	3	28	Q	4.14E-05
	0	29	4	25	1	29	3	27	Q	4.10E-05
	0	28	4	24	1	28	3	26	Q	4.05E-05
	0	27	4	23	1	27	3	25	Q	3.99E-05

	0	44	4	40	1	44	3	42	Q	3.94E-05
	0	26	4	23	1	26	3	23	Q	3.93E-05
	0	26	4	22	1	26	3	24	Q	3.92E-05
	0	45	4	41	1	45	3	43	Q	3.87E-05
	0	25	4	22	1	25	3	22	Q	3.85E-05
998.97	0	19	3	16	1	19	2	18	Q	3.28E-05
	0	18	3	15	1	18	2	17	Q	3.16E-05
	0	21	1	20	1	20	0	20	P	3.07E-05
	0	17	3	14	1	17	2	16	Q	3.04E-05
	0	16	3	13	1	16	2	15	Q	2.90E-05
	0	15	3	12	1	15	2	14	Q	2.76E-05
	0	14	3	11	1	14	2	13	Q	2.61E-05
	0	13	3	11	1	13	2	11	Q	2.46E-05
	0	13	3	10	1	13	2	12	Q	2.45E-05
	0	12	3	10	1	12	2	10	Q	2.29E-05

The strong peak at 1002.10 cm^{-1} was assigned to a hot band. The peak at 1003.50 cm^{-1} is the strongest one in the region of 970-1017 cm^{-1}. It was assigned to Q-branch ν_{26} vibration band of *trans*-1,3-pentadiene. The transitions associated with this peak are presented in Table 6.

Table 6. Transitions assigned to Q-branch ν_{26} at 1003.50 cm^{-1}

Observed frequencies (cm^{-1})	Ground state				Excited state				Branch (P, Q, R)	Intensity in the simulated spectrum
	v	J	K_a	K_c	v	J	K_a	K_c		
1003.50	0	43	0	43	1	43	1	43	Q	0.00016
	0	44	0	44	1	44	1	44	Q	0.00016
	0	42	0	42	1	42	1	42	Q	0.00016
	0	45	0	45	1	45	1	45	Q	0.00016
	0	41	0	41	1	41	1	41	Q	0.000159
	0	46	0	46	1	46	1	46	Q	0.000159
	0	40	0	40	1	40	1	40	Q	0.000159
	0	47	0	47	1	47	1	47	Q	0.000159
	0	39	0	39	1	39	1	39	Q	0.000158
	0	48	0	48	1	48	1	48	Q	0.000158

Four satellite peaks at higher frequency, 1009.42, 1011.18, 1012.88 and 1014.68 cm^{-1} were also matched and assigned to specific transitions. (Table 7)

Table 7. Transitions assigned to four Q-branch peaks at 1009.42, 1011.18, 1012.88 and 1014.68 cm^{-1}

Observed frequencies(cm^{-1})	Ground state				Excited state				Branch (P, Q, R)	Intensity in the simulated spectrum
	v	J	K_a	K_c	v	J	K_a	K_c		
1009.42	0	34	3	31	1	34	4	31	Q	4.36E-05
	0	33	3	30	1	33	4	30	Q	4.35E-05
	0	35	3	33	1	5	4	31	Q	4.33E-05
	0	34	3	32	1	34	4	30	Q	4.33E-05
	0	36	3	34	1	36	4	32	Q	4.33E-05
	0	32	3	29	1	32	4	29	Q	4.32E-05
	0	33	3	31	1	33	4	29	Q	4.32E-05
	0	37	3	35	1	37	4	33	Q	4.31E-05
	0	32	3	30	1	32	4	28	Q	4.30E-05
	0	31	3	28	1	31	4	28	Q	4.29E-05
1011.18	0	37	1	36	1	38	2	36	Q	4.39E-05
	0	38	1	37	1	39	2	37	Q	4.36E-05
	0	37	4	33	1	37	5	33	Q	4.34E-05
	0	37	4	34	1	37	5	32	Q	4.34E-05
	0	36	4	32	1	36	5	32	Q	4.34E-05
	0	36	4	33	1	36	5	31	Q	4.34E-05
	0	38	4	34	1	38	5	34	Q	4.34E-05
	0	38	4	35	1	38	5	33	Q	4.34E-05
	0	35	4	31	1	35	5	31	Q	4.34E-05

	0	35	4	32	1	35	5	30	Q	4.33E-05
1012.88	0	38	5	33	1	38	6	33	Q	4.39E-05
	0	38	5	34	1	38	6	32	Q	4.36E-05
	0	37	5	32	1	37	6	32	Q	4.34E-05
	0	37	5	33	1	37	6	31	Q	4.34E-05
	0	39	5	34	1	39	6	34	Q	4.34E-05
	0	39	5	35	1	39	6	33	Q	4.34E-05
	0	36	5	31	1	36	6	31	Q	4.34E-05
	0	36	5	32	1	36	6	30	Q	4.34E-05
	0	40	5	35	1	40	6	35	Q	4.34E-05
	0	40	5	36	1	40	6	34	Q	4.33E-05
1014.68	0	38	6	32	1	38	7	32	Q	4.04E-05
	0	38	6	33	1	38	7	31	Q	4.04E-05
	0	39	6	33	1	39	7	33	Q	4.04E-05
	0	39	6	34	1	39	7	32	Q	4.04E-05
	0	37	6	31	1	37	7	31	Q	4.03E-05
	0	37	6	32	1	37	7	30	Q	4.03E-05
	0	40	6	34	1	40	7	34	Q	4.03E-05
	0	40	6	35	1	40	7	33	Q	4.03E-05
	0	36	6	30	1	36	7	30	Q	4.02E-05
	0	36	6	31	1	36	7	29	Q	4.02E-05

All observed major peaks in the spectrum of *trans*-1,3-pentadiene were assigned to specific rotational-vibrational transitions.

Conclusions

A quantum cascade laser -based spectrometer was built to obtain high-resolution infrared spectra of *trans*-1,3-pentadiene in the region of 970 to 1017 cm^{-1}. The piezo-scans of *trans*-1,3-pentadiene in the multipass cell were taken simultaneously with those of methanol in the reference cell for calibration. All peaks in the acquired methanol spectra were matched with their corresponding peaks in a reference spectrum, which was generated by SpectraPlot using the HITRAN Database. A fitting curve was used to find the frequencies of all points in a spectrum. After all piezo-scans were calibrated, multiple spectra were combined to obtain a single spectrum of *trans*-1,3-pentadiene. For absorbance calculation, a spectrum of the background was acquired by sweep-scan. A high-resolution absorbance spectrum of *trans*-1,3-pentadiene was obtained in the range of 970-1017 cm^{-1}. The frequency uncertainty, which was estimated as the difference in frequency of overlapping peaks in adjacent spectra, is 0.002 cm^{-1}. Major peaks in the spectrum included: 976.69 (weak), 1002.10 (strong), 1003.50 (very strong), 1009.42 (weak), 1011.18 (weak), 1012.98 (weak) and 1014.68 (weak) cm^{-1}.

By comparing to the vibrational modes reported in the paper by Compton and George, the two peaks at 976.69 and 1003.50 cm^{-1} were assigned to the ν_{18} and ν_{26} bands respectively. Anharmonic vibrational frequencies and rotational constants were calculated using the GAUSSIAN 16 software and specific motions associated with ν_{18} and ν_{26} bands were assigned. A spectrum of *trans*-1,3-pentadiene was simulated using the calculated rotational constants and the values obtained from the study by Hsu and Flygare. Satellite bands of ν_{26} vibrational mode were studied and assigned to specific transitions, which include multiple broad, weak Q-branch peaks at 984.94, 986.67, 988.57, 990.22, 993.69, 995.43, 997.28 and 998.97 cm^{-1}, and four medium to weak peaks at 1009.42,

1011.18, 1012.88 and 1014.68 cm^{-1}. The strong peak at 1002.10 cm^{-1} which was not observed in the simulated spectrum was assigned to the hot band of ν_{26} transition.

The experiment can be improved by the development of a new system to prepare samples so isoprene can be removed from the spectrum.

References

1. Liu, K.; He, Q.; Renm, L.; Gong, L.J.; Hu, J.L.; Ou, E.C, Xu, W.J. *Synthesis and characterization of the well-defined polypentadiene via living anionic polymerization of (E)-1,3-pentadiene.* 2016. Polymer 89: 28-40.

2. Liang, Y.; Luo, Y.Y.; Jing, W.; Chen, K.; Zhao, P.F.; Li, P.W.; Zhang, B.L. *A py-GC/MS technique for structural elucidation of rubber samples to investigate regional effects on bio-coagulated natural rubber.* 2017. Journal of Analytical and Applied Pyrolysis 123: 118-125.

3. Zieba-Palus, J.; Nowinska, S.; Kowalski, R. *Application of infrared spectroscopy and pyrolysis gas chromatography for characterisation of adhesive tapes.* 2016. Journal of Molecular Structure 1126: 232-239.

4. Medeiros, E.A.; Nicodem, D.E.; Corrêa, R.J. *A new fast methodology to measure total diene content in gasoline. 2011*. Fuel 90: 1696-1699.

5. Nascimento, P.C.; Hilgemann, M.; Guterresl, M.V.; Carvalho, L.M.; Bohrer, D. *Chemometric approach to assess the diene value in hydrogenated pyrolysis gasoline by voltammetry.* 2007. Chemometrics and Intelligent Laboratory Systems 89: 97-101.

6. Compton, D.A.C; George, W.O.; Maddams, W.F. *Conformations of Conjugated Hydrocarbons. Part 2. A Spectroscopic and Thermodynamic Study of cis- and trans-penta-1,3-diene.* 1977. Journal of Chemical Society, Perkin Transaction.2 10: 1311-1315.

7. Hsu, S.L.; Flygare, W.H. *Microwave Spectra, Barriers to Internal Rotation of the Methyl Group, and Molecular Electrical Dipole Moments in trans- and cis-l,3-Pentadiene.* 1969. Journal of Chemical Physics 52: 1053-1057.

8. Nasim, H.; Jamil, Y. *Diode lasers: From laboratory to industry*. 2014. Optics and Laser Technology 56: 211-222.

9. Tino, G.M. *Atomic spectroscopy with diode lasers*. 1994. Physica Scripta 51: 58-66.

10. Nasim, H.; Jamil, Y. *Recent advancements in spectroscopy using tunable diode lasers.* 2013. Laser Physics Letter 10-4 043001.

11. Faist, J.; Capasso, F.; Sivco, L.; Hutchinson, A.L.; Sirtori, C.; Cho, A.Y. *Quantum cascade laser: A new optical source in the mid-infrared.* 1995. Infrared Physics & Technology 36: 99-103.

12. Hamadou, A.; Thobel, J.L.; Lamari, S. *Dynamic modeling of a terahertz quantum cascade laser based on difference frequency generation.* 2018. Optik - International Journal for Light and Electron Optics 156: 595-605.

13 Pyataev, M.A.; Shorokhov, A.V.; Khvastunov, N.N.; Vlasov, K.R.; Krevchik, V.D.; Semenov, M.B.; Alekseev, K.N.; Kusmartsev, F.V. *Amplification of electromagnetic radiation in a superlattice placed in a tilted magnetic field.* 2017. Nanosystems: Physics, Chemistry, Mathematics 8-6: 717-722.

14. Ko¨hler, R.; Tredicucci, A.; Beltram, F.; Beere, H.E.; Linfield, E.H.; Davies, A.G.; Ritchie, D.A.; Lotti, R.C.; Rossi, F. *Terahertz semiconductorheterostructure laser*. 2002. Nature 417: 156-159.

15. Waried, H.H. *Synchronization of quantum cascade lasers with mutual optoelectronic coupling*. 2018. Chinese Journal of Physics 56-3: 1113-1120.

16. Vallon, R.; Parvitte, B.; Bizet, L.; Naurois, G.M.D.; Simozrag, B.; Misons, G.; Carras, M.; Zeninari, V. *External cavity coherent quantum cascade laser array.* 2016. Infrared Physics & Technology 76: 415-420.

17. McQuarrie, D.A.; Simon, J.D. *Physical Chemistry A Molecular Approach*. 1997. University Science Books: 157-178, 495-536.

18. Bernath. P.F. *Spectra of Atoms and Molecules 2nd Edition.* 2005. Oxford University Press: 182-286.

19. Struve, W.S. *Fundamentals of Molecular Spectroscopy.* 1989. John Wiley & Sons, Inc: 73-97.

20. Tamura, K.; Nanko, T.; Takamatsu, Y.; Matsuo, J. *TDLS200 Tunable Diode Laser Gas Analyzer and its Application to Industrial Process.* 2010. Yokogawa Technical Report English Edition 53-2: 113-116.

21. Goldestein, C.S.; Miller, V.A.; Spearrin, R.M.; Strand, C.L. *SpectraPlot.com: Integrated spectroscopic modeling of atomic and molecular gases.* 2017. Journal of Quantitative Spectroscopy & Radiative Transfer 200: 249-257.

22. Rothman, L.S.; Gordon, I.E.; Babikov, Y.; Barbe, A.; Chris Benner, D.; Bernath P.F.; Birk, M.; Bizzocchi, L.; Boudon, V.; Brown, L.R.; Campargue, A.; Chance, K.; Cohen, E.A.; Coudert, L.H.; Devi, V.M.; Drouin, B.J.; Fayt, A.; Flaud, J.M.; Gamache, R.R.; Harrison, J.J.; Hartmann, J.M.; Hill, C.; Hodges, J.T.; Jacquemart, D.; Jolly, A.; Lamouroux, J.; Le Roy, R.J.; Li, G.; Long, D.A.; Lyulin, O.M.; Mackie, C.J.; Massie, S.T.; Mikhilenho, S.; Muller, H.S.P.; Naumenko, O.V.; Nikitin, A.V.; Orphal, J.; Perevalov, V.; Perrin, A.; Polovtseva, E.R.; Richard, C.; Smith, M.A.H.; Starikova, E.; Sung, K.; Tashkun, S.; Tennyson, J.; Toon, G.C.; Tyuterev, V.G.; Wagner. *The*

HITRAN2012 molecular spectroscopic database. 2013. Journal of Quantitative Spectroscopy & Radiative Transfer 130: 4-50.

23. Frisch, M.J.; Trucks, G.W.; Schlegel, H.B.; Scuseria, G.E.; Robb, M.A.; Cheeseman, J.R.; Scalman, G.; Barone, V.; Petersson, G.A.; Nakatsuji, H.; Li, X.; Caricato, M.; Marenich, A.V.; Bloino, J.; Janesko, B.G.; Gomperts, R.; Mennucci, B.; Hratchian, H.P.; Ortiz, J.V.; Izmaylov, A.F.; Sonnenberg, J.L.; Williams-Young, D.; Ding, F.; Lipparini, F.; Egidi, F.; Goings, J.; Peng, B.; Petrone, A.; Henderson, T.; Ranasinghe, D.; Zakrzewski, V.G.; Gao, J.; Rega, N.; Zheng, G.; Liang, W.; Hada, M.; Ehara, M.; Toyota, K.; Fuduka, R.; Hasegawa, J.; Ishid, M.; Nakajima, T.; Honda, Y.; Kitao, O.; Nakai, H.; Vreven, T.; Throssell, K.; Montgomery Jr., J.A.; Peralta, J.E.; Ogliaro, F.; Bearpark, M.J.; Heyd, J.J.; Brothers, E.N.; Kudin, K.N.; Staroverov, V.N.; Keith, T.A.; Kobayashi, R.; Normand, J.; Raghavachari, K.; Rendell, A.P.; Burant, J.C.; Iyengar, S.S.; Tomasi, J.; Cossi, M.; Millam, J.M.; Klene, M.; Adamo, C.; Cammi, R.; Ochterski, J.W.; Martin, R.L.; Morokuma, K.; Farkas, O.; Foresman, J.B.; Fox, D.J. *Gaussian 16 Software Package, Revision A. 03.* 2016.

24. Barone, V. *Anharmonic vibrational properties by a fully automated second-order perturbative approach. 2005.* Journal of Chemical Physics 122- 014108.

25. Western,C. *PGOPHER, A Program for Simulating Rotational Structure.* 2010.